Available online at www.sciencedirect.com
ScienceDirect
Journal of Power Sources 159 (2006) 781–801
JOURNAL OF POWER SOURCES
www.elsevier.com/locate/jpowsour

Review

Hydrogen storage by carbon materials☆

R. Ströbel[a,*], J. Garche[b], P.T. Moseley[c], L. Jörissen[b], G. Wolf[d]

[a] *Reinz-Dichtungs-GmbH, Reinzstraße 3-7, D-89233 Neu-Ulm, Germany*
[b] *Center for Solar Energy and Hydrogen Research Baden-Wuerttemberg, Helmholtzstr. 8, D-89075 Ulm, Germany*
[c] *International Lead Zinc Research Organization Inc., P.O. Box 12036, Research Triangle Park, NC 27709, USA*
[d] *TU Freiberg Institut für Physikalische Chemie, Leipziger Straße 29, D-09596 Freiberg, Germany*

Available online 30 June 2006

Abstract

In order for fuel cells to become a practical means of supplying power for road vehicles it will be necessary for a viable method of on-board hydrogen storage to be identified and implemented. Target values that must be achieved for the critical parameters in such a system have been drawn up by the US Department of Energy. It is quite clear that these targets cannot be met by systems that store hydrogen at high pressure or as a liquid at cryogenic temperatures. Attention has thus been focused on methods of storing hydrogen in, or on, a solid phase. In such schemes it is obviously desirable to make use of elements from the early part of the periodic table and there has been much interest in the possible use of carbon as a hydrogen host. This paper provides an overview of experimental work on such systems together with an outline of theoretical studies that have been undertaken to estimate the practical limits to the amount of hydrogen that could be stored per unit weight.

Keywords: Hydrogen; Storage; Carbon; Materials; Methods

Contents

☆This review is one of a series dealing with the role of carbon in electrochemical energy storage. The reviews covering the role of carbon in fuel cells and the role of carbon in graphite and carbon powders were published in *J. Power Sources*, volume 156, issue 2, pages 128–150. The reviews covering the role of carbon in valve-regulated lead-acid battery technology and carbon properties and their role in supercapacitors were published in *J. Power Sources*, volume 157, pages 3–27.

* Corresponding author.
E-mail addresses: raimund.stroebel@dana.com (R. Ströbel), juergen.garche@zsw-bw.de (J. Garche), pmoseley@ilzro.org (P.T. Moseley), gert.wolf@chemie.tu-freiberg.de (G. Wolf).

0378-7753/$ – see front matter © 2006 Elsevier B.V. All rights reserved.
doi:10.1016/j.jpowsour.2006.03.047

1. Introduction

Hydrogen storage is an essential prerequisite for the widespread deployment of fuel cells, particularly in transport. The US Department of Energy (DOE) has announced a 6.0 wt% target for hydrogen storage on-board automobiles (2010). None of the known storage methods (compression, liquefaction, or storage as metal hydrides), however, can meet these targets. Compressed and/or liquid hydrogen is currently used in fuel cell powered automobiles but application issues, such as safety and the need for a hydrogen supply infrastructure, are problems which remain to be solved. Solid-state hydrogen storage systems, such as metal hydrides, chemical hydrides, or hydrogen-absorbing carbon materials, are expected to be simpler for the engineering design of vehicles and considerably safer than the storage of elemental hydrogen (Fig. 1).

Unfortunately these solid-state systems, including those forms of carbon that have been known for a long time, do not meet the DOE targets, either. Following the development of carbon nanostructures, such as fullerene, nanofibers, and other forms discovered since 1985, however, new possibilities for efficient hydrogen storage have emerged. The DOE has asked for achievable hydrogen storage capacity to reach 4.5 wt% by the FY 2005, 6.0 wt% by the FY 2010, and 9.0 wt% by the FY 2015. The different time-dependent DOE targets are shown in Table 1.

In early publications, e.g. Rodriguez and co-workers [3], huge hydrogen storage capacities, up to 67%, were reported. Unfortunately such astonishing values could not confirmed by other research teams worldwide. Nevertheless, this publication stimulated a considerable increase in R&D activity in the field of hydrogen storage in carbon nanomaterials.

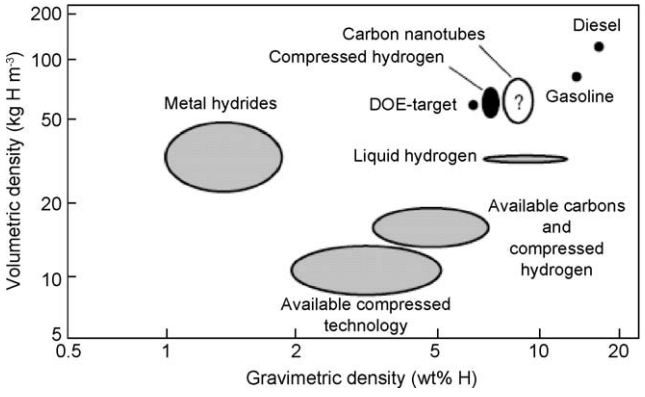

Fig. 1. Volumetric and gravimetric hydrogen density for different storage methods [1].

This review provides an overview of the basics of hydrogen storage on carbon materials, the types of carbon materials with potential for hydrogen storage, the measured hydrogen storage capacities of these materials, and, based on calculations, an approximation of the theoretical achievable hydrogen storage capacity of carbon materials.

2. Carbon materials

2.1. Activated carbon

Activated carbon (AC) is a synthetic carbon modification containing very small graphite crystallites and amorphous carbon. The pore diameters are usually less than 1 nm and form a specific surface up to 3000 $m^2\ g^{-1}$.

AC is prepared from carbon-rich organic precursors by a thermal method (dry distillation) to form carbonized organic precursors, which can be activated to increase the pore volume either thermally or chemically:

Thermal method: Treatment at ~700–1000 °C in the presence of oxidizing gases such as steam, CO_2, steam/CO_2 mixtures, or air.
Chemical method: Treatment at ~500–800 °C in the presence of dehydrating substances such as $ZnCl_2$, H_3PO_4, or KOH, which are leached out afterwards.

Table 1
DOE targets for hydrogen on-board storage and specific data for a 5 kg H_2 system [2]

Storage parameter	2005	2010	2015
Gravimetric capacity (specific energy) (kW h kg^{-1})	1.5	2.0	3.0
Gravimetric capacity (specific energy) (kg H_2 kg^{-1})	0.045	0.060	0.090
System weight (kg)	111	83	55.6
Volumetric capacity (energy density) (kW h l^{-1})	1.2	1.5	2.7
Volumetric capacity (energy density) (kg H_2 l^{-1})	0.036	0.045	0.081
System volume (l)	139	111	62
Storage system cost (US$ kW h^{-1})	6	4	2
System cost (US$)	1000	666	333
Refueling rate (kg H_2 min^{-1})	0.5	1.5	2.0
Refueling time (min)	10	3.3	2.5

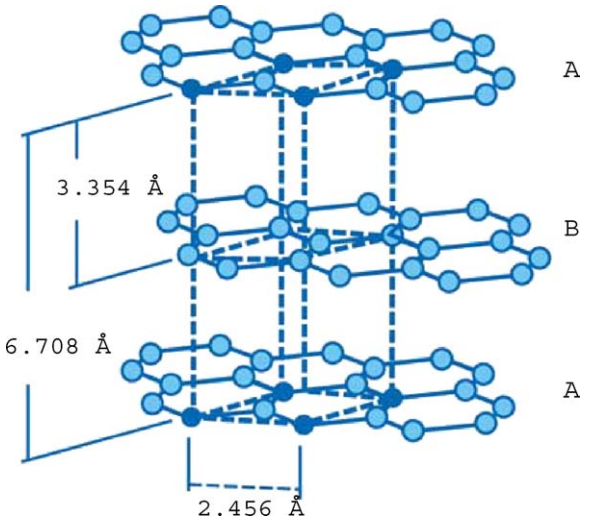

Fig. 2. Graphite structure.

A good overview of activated carbon preparation is given by Marsh and Rodriguez-Reinoso [4,5].

2.2. Graphite

Graphite is one of the four ordered carbon allotropes (diamond with sp^3-bonding, graphite with sp^2-bonding, fullerene with perturbed sp^2-bonding, and carbyne with sp^1-bonding). Graphite has a sheet-like structure where the atoms all lie in a plane and are only weakly bonded, via van der Waals forces, to the graphite sheets above and below. It has a perfect basal cleavage (Fig. 2).

Graphite is a naturally occurring mineral with up to 20 wt% impurities. Graphite can also be made artificially, usually by heating petroleum coke or coal pitch at very high temperatures ~2500 °C.

2.3. Graphene

Graphene is not an allotrope of carbon, it is a single planar sheet of sp^2 bonded carbon atoms, identical to one of the layers of the graphite structure but isolated. The sheet is of finite size and other elements can appear at the edge of the sheet. A typical graphene sheet has the chemical formula $C_{62}H_{20}$, where the hydrogen is used to terminate the dangling bonds. Graphenes are aromatic.

Graphenes are normally formed only of hexagonal cells. If a pentagonal cell is present then the plane warps into a conical shape. The insertion of 12 pentagons can lead to the formation of a 'fullerene' (see Section 2.4.1).

Planar graphene itself has been presumed not to exist in the free state, as it would be unstable with respect to the formation of curved structures such as soot, fullerenes, and nanotubes. Nevertheless, attempts have been made to isolate a single graphene sheet by mechanical exfoliation (repeated peeling) of small fragments of highly oriented pyrolytic graphite, in order to study the electrical properties of graphene. An electron and hole mobility of up to 10^4 cm^2 V^{-1} s^{-1} has been reported [6].

2.4. Carbon nanostructures

2.4.1. Fullerene

Fullerenes were first observed in molecular beam experiments, where discrete peaks were found corresponding to C_{60} and C_{70} molecules by Kroto et al. [7].

Fullerenes are a class of carbon molecules in which the carbon atoms are arranged into 12 pentagonal faces and 2 or more hexagonal faces. The fullerene structure can be understood (although not practically manufactured this way) as a rolled up single layer of graphene. Whereas graphite is built up of many graphene sheets of linked hexagonal carbon atoms, the fullerenes are formed by pentagonal (or sometimes heptagonal) carbon rings, which prevent the formation of planar structures. These fullerene molecules can take the form of spheres, ellipsoids, or tubes.

Spherical fullerenes are often referred to as 'buckyballs', and cylindrical fullerenes as 'buckytubes' or 'nanotubes'.

The names fullerene, buckyball, and buckytube refer to the architect Richard Buckminister-Fuller, who popularized the geodesic dome (shaped like an incomplete buckyball). In fact this structure had already been used in 1913 by Carl Zeiss in Jena for its planetarium dome.

Both the spherical and the cylindrical fullerenes are hollow. The smallest possible complete fullerene molecule could be built up from 32 carbon atoms.

Fullerenes are formed when carbon is vaporized (e.g. by a pulsed laser, or an arc discharge), mixed with an inert gas, and then slowly condensed. If metal catalysts are included in the process nanotubes are formed. If not, then spherical fullerenes are formed.

The production of pure C_{60} in large quantities has been described by Krätschmer et al. [8]. Fullerenes can also be found in ordinary candle soot.

An overview of fullerenes and nanotubes is given in references [9,10].

2.4.1.1. Spheres. By far the most common fullerene is C_{60}. Many others, e.g. C_{70}, C_{76}, and C_{84} or even C_{240}, and C_{540}, are well known too.

The C_{60} molecule consists of 60 carbon atoms, which are bonded in a nearly spherical configuration. This shape, which is similar to a soccer ball, is called a truncated icosahedron with 20 hexagons and 12 pentagons. This molecule is the archetypal Buckminster-fullerene or buckyball.

Its diameter is about 7 Å. It is a powder, with yellow color and is soluble (the only carbon allotrope to be so) in certain solvents, e.g. toluene and carbon disulfide. Solutions of pure Buckminster-fullerene have a deep purple color.

Additives which are built into fullerenes are placed either between the balls or inside the balls (endohedral fullerenes). An inside trap is easier with larger fullerenes such as those with 82 or more carbon atoms. When the atom(s) trapped inside are metallic, the molecules are referred to as metallofullerenes. If three alkali atoms are added per C_{60} the fullerene becomes superconducting at about 10–40 K, depending on the alkali type.

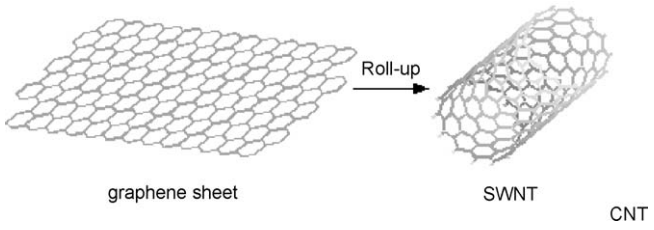

Fig. 3. Scheme of the structure of a carbon nanotube (although note that the nanotube cannot actually be prepared by 'rolling up' a graphene sheet).

An overview of this kind of fullerene is given by Margadonna and Prassides [11].

2.4.1.2. Carbon nanotubes (CNT). After the discovery of the Buckminister-fullerene (C_{60}) in 1985 the discovery of nanotubes (in 1991 [12–14]) was only a question of time.

As mentioned above, each CNT can be envisaged as a cylindrical rolled single layer of graphene (Fig. 3).

Because a graphene sheet can be formed into a tube in different ways, different types of carbon nanotubes exist, namely 'armchair', 'zigzag', and 'chiral' types (Fig. 4).

The quasi-rolling direction, quantified by the 'chiral vector', determines the electrical nature of the CNT, i.e. whether it behaves as a conductor or a semiconductor. The mechanical parameters are also influenced by the rolling direction. A Young's modulus of over 1 TPa, and a tensile strength of about 200 GPa can be achieved.

The 'rolling' up of the graphene sheets is not only limited to one sheet. A plurality of sheets could be rolled up, to form 'multiwall nanotubes' (MWNTs) instead of the one-layer structure 'single-wall nanotube' (SWNT).

The first nanotubes to be discovered (Iijima [12]) were in fact MWNTs. It was two years later that Iijima and Ichihashi [13] and Bethune et al. [16] reported the synthesis of SWNTs.

The MWNT is an arrangement of coaxial tubes of graphene sheets forming a tube-like structure. Each MWNT has from 2 to 50 such tubes. The structure of the MWNT could be envisaged as being like a set of Russian dolls, contained inside one another.

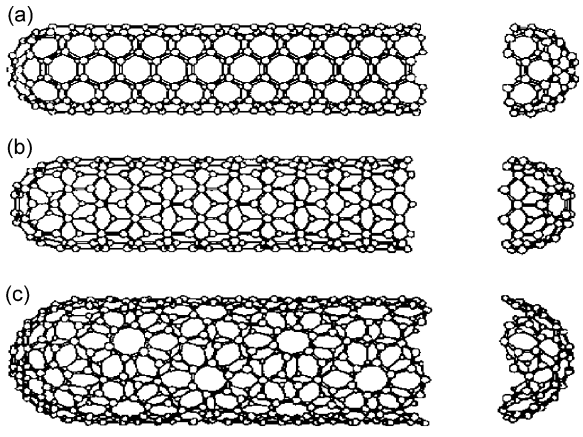

Fig. 4. Scheme of the different single-walled nanotube (SWNT) structures: (a) armchair, (b) zigzag, and (c) chiral [15].

SWNTs have a diameter of around 1 nm. MWNT have inner diameters from 1.5 to 15 nm and outer diameters from 2.5 to 30 nm. The interlayer distance of the MWNT amounted to 0.34–0.36 nm, i.e. similar to the interlayer distance in graphite. SWNTs and MWNTs are usually several micrometers in length.

MWNTs are frequently constituted of tilted or conical tubes that closely resemble the structure of 'herringbone structure' graphite nanofibers (GNFs) which are described in Section 2.4.2. Indeed the terms MWNT and GNF are sometimes used interchangeably.

CNTs are formed by the evaporation of bulk carbon to generate carbon molecules and atoms, which afterwards condense as CNTs [17].

The evaporation sources can be any one of the following:

(i) *Arc discharge* [18]: An arc discharge between two carbon electrodes with or without a catalyst. Large quantities of impure CNTs are produced in this way.
(ii) *Laser ablation*: A pulsed or continuous Nd YAG laser impinges on a graphite target, which is placed in an oven at 1200 °C and 500 Torr of argon or helium. If the target consists of graphite mixed with cobalt, nickel, or iron SWNTs are formed. If a pure graphite target is used MWNTs are produced.
(iii) *Chemical vapor deposition*: CVD with 3d metal catalysts, e.g. ferrocene, forms mainly MWNTs. A smaller fraction of the product comprises SWNTs but these have a poor quality, e.g. a large diameter range. The catalyst has a large influence on the product [19].

The synthesis of CNTs is usually not very selective. Normally the ends of the CNTs are closed by fullerene-like hemispherical structures. The tubes could be opened via a chemical (e.g. HNO_3) or ultrasound treatment. Open CNTs can be closed by thermal treatment.

A review of such processes is given by Khare and Bose [20].

2.4.2. Carbon nanofibers (CNF) and graphite nanofibers

Nanofibers were first observed (in about 1970) during a study of the catalytic dehydrogenation of hydrocarbons, where it was found that they caused a deactivation of the catalyst. This was the starting point for an intensive investigation of carbon nanofibers. Whereas Fullerenes and nanotubes are hollow, nanofibers are not.

CNF structures are formed at high temperatures from a mixture of carbon-containing gases and hydrogen, or from hydrocarbons alone, on catalysts comprising mostly nickel- and iron-based alloys. Depending on the nature and shape of the catalyst, the ratio of the hydrocarbon/hydrogen reactant mixture, and the reaction conditions, different types of CNF could be formed. Specifically, these differ in morphology, crystallinity, and shape.

The key steps in the nanofiber formation process can be explained by reference to Fig. 5.

Hydrocarbon is adsorbed on the surface, A, of the catalyst particle, B. Carbon–carbon bonds are broken. A carbon atom

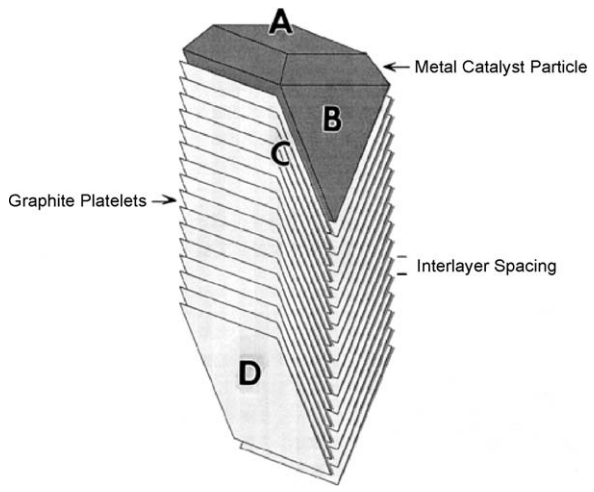

Fig. 5. Scheme of a carbon nanofiber with a catalyst particle [21].

diffuses to the interface, C, between the catalyst particle and the platelets, D, to form a carbon nanostructure.

The as-grown fibers consist of the carbon nanofiber and the catalyst particle. The as-grown fibers can be purified by leaching the catalyst with acid.

The platelets that are formed are mainly graphite [22,23]. Therefore, the term 'graphite nanofiber' is used in parallel to the term 'carbon nanofiber'. But depending on the catalyst crystal faces, less-ordered carbon may also grow [24].

The arrangement of the graphite platelets depends on the geometry of the catalyst. The platelets are structured according to the catalyst shape over a large number of platelet layers. Different shapes of CNF are shown in Fig. 6.

The fibers are usually between 5 and 100 μm in length, and their diameter is between 5 and 100 nm. The specific surface areas (BET) of these ordered crystalline solids are normally between 100 and 300 $m^2\,g^{-1}$ but can sometimes reach values up to 700 $m^2\,g^{-1}$. In the 'herringbone' structure the graphite layers are separated from one another by a distance of 3.4 Å.

The structure of the platelets provides many edges on a nanofiber which represent a large surface, with many interaction sites for adsorbates.

A good review of carbon nanofibers has been published by Baker [21].

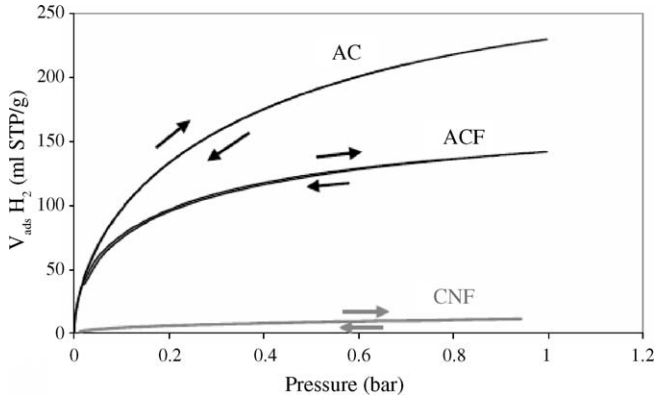

Fig. 7. Adsorption isotherms for activated carbon (AC), activated carbon fibers (ACF), and carbon nanofibers (CNF) [33].

3. Hydrogen storage fundamentals

3.1. Physisorption

Physisorption is based on the van der Waals interaction (a resonant fluctuation in the charge distribution) between gases and solids. The interaction energy, also called the London-Dispersion forces (E_{S-H_2}), between the substrate (S) and the hydrogen molecule (H_2), is given by

$$E_{S-H_2} \sim \frac{\alpha_{H_2}\alpha_S}{R^6} \quad (1)$$

where α is the polarizibility and R is the interaction distance. Because α_{H_2} is fixed, the only way to increase E_{S-H_2} is to use highly polarizable substrates, e.g. substrates with π-electron systems.

The equilibrium between gas attraction and gas repulsion on the surface creates an energy minimum which amounts to between 1 and 10 kJ mol^{-1}. The exact value for the hydrogen adsorption on a flat carbon surface depends on the adsorption stereometry. An average value would be about 4–5 kJ mol^{-1}. This represents a very weak interaction. Therefore, hydrogen is desorbed with increasing temperature, and very little hydrogen adsorption is observed on carbon at elevated temperatures.

Normally only a monolayer is adsorbed above the boiling point of the adsorbant [26]. In this case the Langmuir isotherm should apply. Fig. 7 shows the adsorption isotherms for three different carbon materials.

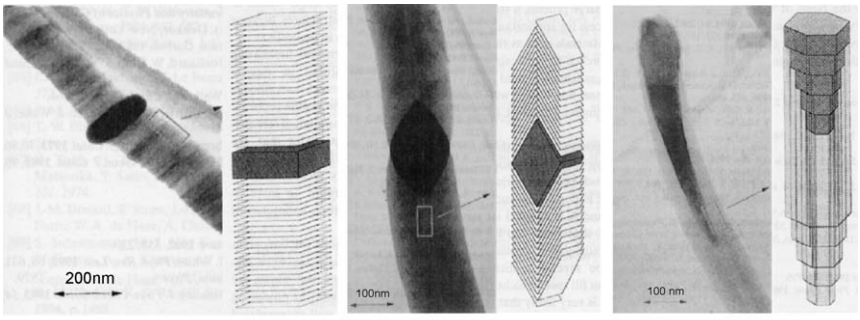

Fig. 6. Different structures of carbon nanofibers (CNFs): (A) deck of cards structure, (B) herringbone structure, and (C) tubular structure [25].

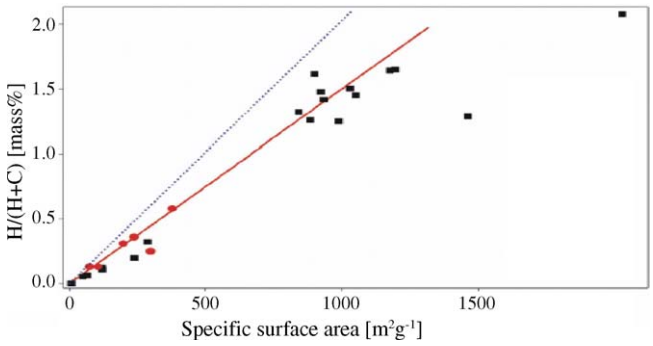

Fig. 8. Reversible amounts of hydrogen adsorbed vs. surface area [27]. (Circles) Carbon nanotubes, high surface area graphite (electrochemical measurement at 298 K). (Squares) Hydrogen adsorption measurement at 77 K from Nijkamp et al. [28]. (Dotted line) Calculated amount of hydrogen in a monolayer at the substrate surface.

From this diagram it is evident that reversible physisorption takes place with all samples.

The maximum value of hydrogen adsorption on any particular material can be estimated as the quantity of hydrogen that can be accommodated in a monolayer [27]. With the assumption that the structure of the adsorbed hydrogen is closed-packed face-centered, the minimum surface area for the adsorption of 1 mol of hydrogen amounts to S_{ml} (H_2) = 85.917 m^2 mol^{-1}. Based on the surface area of a single graphene sheet (1315 m^2 g^{-1}) the maximum value for the storage capacity of hydrogen adsorbed on graphite is calculated to be about 3 wt%. This value, however, can be reached only at very low temperatures.

Based on this approximation the theoretical hydrogen storage capacity (m_{ads}) can be calculated from the specific surface of the carbon (S_{spec}): $m_{ads} \approx S_{spec} \times 2.27 \times 10^{-3}$ wt%; the amount of adsorbed hydrogen correlates with the specific surface of carbon. Taking this equation into account a theoretical carbon surface area of 2600 m^2 g^{-1} would be necessary to meet the 2010 DOE target (6 wt%).

Fig. 8 shows the experimental relationship between different carbon surfaces and the hydrogen storage capacity under different measurement conditions.

An extrapolation shows that the 2010 DOE target (6 wt%) would be reached at a carbon surface of >4000 m^2 g^{-1}. This is not yet available.

Activated carbons have relatively high surface areas. Bulk graphite, with its relatively high polarizibility α_S (see Eq. (1)), caused by its π-electron system, should show a good hydrogen storage. Extrapolated ab initio (MP2) computations [29] found a physisorption energy for hydrogen on graphene sheets of 7.2 kJ mol^{-1}. But this value will be reduced, by the entropy contribution (3.4 kJ mol^{-1}) and a penalty due to lower binding energies of different orientations and adsorption sides, to about 2.5 kJ mol^{-1} at room temperature (a convenient temperature for practical hydrogen storage) [29].

But the interlayer distance in graphite (3.354 Å) is too small for the intercalation of free hydrogen molecules with a dynamic diameter of 4.06 Å. Furthermore the specific surface area of bulk graphite is too low and therefore a practically hydrogen uptake can not be observed [30].

An expansion of the interlayer distance of graphite, and a corresponding increase in specific surface area, are possible via:

(i) *Enlargement of the distance between the graphene sheets* by intercalation of, e.g. alkali metals and metal halides [31,32]. An enlargement of the d-spacing to 10 Å is expected [33], based on calculations [34–36].
(ii) *Graphite nanofibers*, which are an arrangement of graphene platelets in a parallel, perpendicular, or angled orientation with respect to the fiber axis. The many edges of the platelets provide a large surface with many interaction sites for adsorbates.
(iii) *Graphite nanotubes*, which could be pictured as rolled up graphene sheets, with enhanced adsorption sites between pseudographitic layers, and on interstitial sites, both inside and outside the tube.
(iv) *Ball milling graphite*; the ball milling leads to an enormous increase in specific surface area by reducing the size of the fundamental particles.
(v) *Carbon foams* with an unusual structure based on rigidly interconnected segments of graphite. This hypothetical new system might be formed by a hierarchical self-assembly process from nanostructured graphite. The resulting "foam" covers the structural phase space extending from hexagonal diamond (lonsdaleite) to graphite [37,38]. Furthermore metal nanoparticles can be relatively easily incorporated in order to catalyze the formation of graphitic structures [39].

Besides the high polarizability and the high surface areas, adsorption can be increased by a curving of the structure of the carbon surface. This curved structure leads to an overlap of the potential fields of carbon atoms and therefore to an increase of the adsorption energy — up to 30 kJ mol^{-1} [40].

Curved carbon structures are formed in:

(i) *Activated carbons* with micropores [41], where the pore diameter is in the region of the molecular diameter. In this case the potential fields of the different pore wall sides can strongly overlap. Activated carbon normally has a wide pore-size distribution and therefore only a fraction of the pores are able to exhibit the favorable overlap. Pores with a diameter of approximately 0.5–1.0 nm are most beneficial [33]. The relationship between average pore diameter and hydrogen adsorption is shown in Fig. 9.

Therefore, the micropore volume correlates better with the hydrogen storage capacity than does the specific surface area of the carbon.

(ii) *Carbon nanotubes* with a diameter of around 1 nm. For SWNT Heben and co-workers found an unexpectedly high activation energy for hydrogen desorption of 19.6 m^2 g^{-1} [43]. From the Feynman–Hibbs effective potential [44] approximation, it was calculated that the adsorption energy for adsorbed hydrogen at a CNT [45] should be about 9 kJ mol^{-1} at 50 K. This curvature effect is particularly marked at low temperatures. At 50 K, 55 times more hydrogen can be adsorbed on a curved surface than on a flat one.

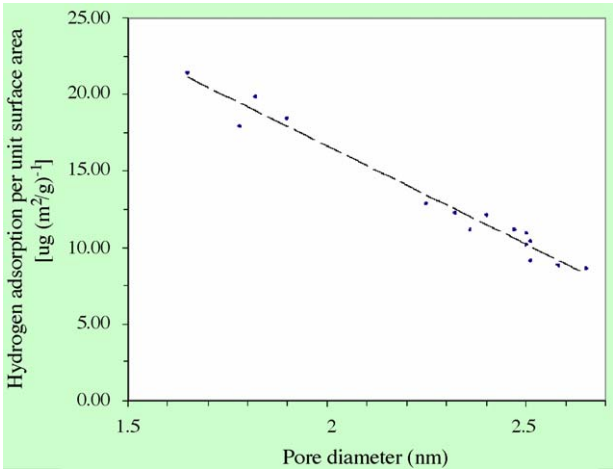

Fig. 9. Hydrogen adsorption (μg of hydrogen per $m^2\,g^{-1}$) vs. average pore diameter of activated PEEK carbons [42].

This factor, however, reduces to 11 when the temperature is raised to 77 K [46]. The adsorption energy, and therefore the hydrogen capacity, depends on several different parameters such as the diameter of the tubes, the chirality of the tubes, and the type of adsorption site. Green's-function Monte Carlo studies of carbon nanotube bundles showed adsorption energies for endohedral sites in the internal channels of 11 kJ mol^{-1}, followed by the grooves (9 kJ mol^{-1}) and surfaces (6 kJ mol^{-1}) on the outer surface of the bundles, and the sites inside the tube with only 5 kJ mol^{-1} [47] (see Fig. 10).

It has been speculated [48] that, for carbon nanotubes, besides the overlapping of the potential fields there might also be an increase in hydrogen storage capacity due to capillary storage, where several layers of hydrogen could condense inside the tube and even between carbon crystal platelets. Under the influence of capillary forces hydrogen should shrink from an effective gas diameter (square root of the product of gas collision and kinetic diameter) of 2.6 Å to about 1.28 Å. So the idea was to draw on the capillary forces at ambient temperatures to achieve a hydrogen storage capacity equivalent to filling the carbon nanotubes with liquid hydrogen. Based on this liquid-like state of the hydrogen at room temperature no refrigeration would be necessary. Up to now, however, no evidence for this effect has been found.

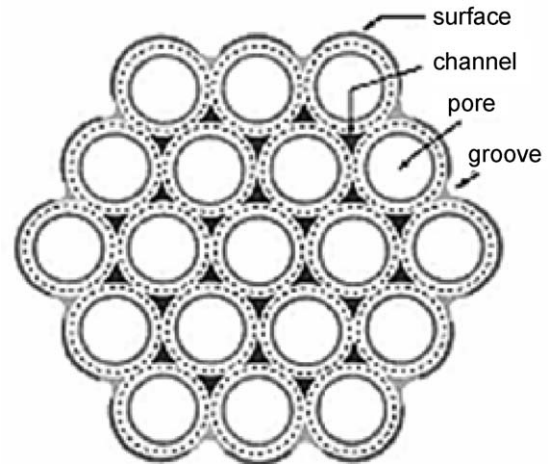

Fig. 10. Different storage sites on MWNTs.

(iii) *Carbon aerogels* (*CA*) have nanostructures and curved surfaces. Metal-doped CAs are a focus for DOE-research [39].

3.1.1. Temperature and pressure influence

The principal influences of pressure and temperature on hydrogen uptake are shown schematically in Fig. 11.

The dependence of hydrogen uptake on pressure and temperature is described by the Langmuir relation; at a constant coverage of hydrogen, with $E_{ad} = E^*_{des} - E^*_{ad}$,

$$\left(\frac{\partial \ln p}{\partial 1/T}\right)_\theta = \frac{E_{ad}}{R} \tag{2}$$

The amount of hydrogen adsorbed decreases with increasing temperature and decreasing pressure. With increasing pressure (up to MPa) a linear increase of the hydrogen adsorption has been observed [49].

Physisorption on carbon nanotubes at cryogenic temperatures and 12 MPa is capable of storing up to 8 wt% of hydrogen. At room temperature this value drops by an order of magnitude to around 0.7 wt%.

3.2. Chemisorption

If the π bonding between carbon atoms were to be fully utilized, every carbon atom could be a site for chemisorption of one hydrogen atom [50,51]. It has been found that hydrogen molecules react with buckyball fullerenes under high pressure (50–3000 MPa) at elevated temperature (500–600 K) [52,53]. Desorption results [54] of nanotubes treated with hydrogen under high pressure show a peak at temperatures above 400 K, which indicates chemisorption. This is ascribed to a complete layer of chemisorbed hydrogen on the outside wall of the nanotube [55,56].

A first-principle calculation shows that a dissociative chemisorption of hydrogen on carbon nanotubes should be possible. The H–H bond breaking (bonding energy 4.52 eV) is concerted with the formation of two C–H bonds on two adjacent nanotubes in the solid phase, and is facilitated by the application of high pressure which shortens the distance between nanotubes [57] from a distance of 1.2 nm at atmospheric pressure to about 1.05 nm at high pressure. This leads to a shortening of the C–C separation between two adjacent tubes from 3.8 to 2.6 Å, and this facilitates dissociative hydrogen adsorption.

The chemisorbed hydrogen, however, can only be released at higher temperatures. Thus, chemisorption is not useful for the practical storage of hydrogen.

3.3. Adsorption energy

An important parameter for the characterization of hydrogen storage is the adsorption energy, ΔE (ads).

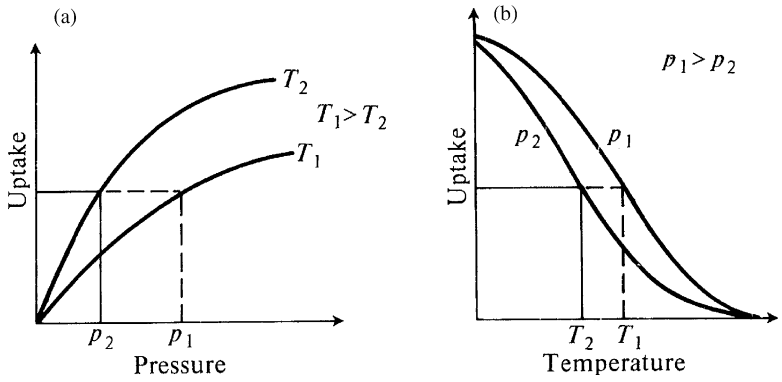

Fig. 11. Schematic view of the influence of (a) pressure and (b) temperature on hydrogen uptake.

If the adsorption energy is low, i.e. we have a weak interaction between hydrogen and carbon, hydrogen will desorb spontaneously at low temperatures. Then hydrogen storage at ambient temperature would only be possible at high pressure.

If the adsorption energy is high, a relative large amount of hydrogen could be adsorbed, but the adsorbed hydrogen would not readily desorb, and only a small amount of fuel would be available.

It would be useful to be able to design a sorbent that adsorbs strongly but whose interaction potential could be attenuated when hydrogen was to be desorbed. Charged carbon nanotubes could form such a system. The charge–quadrupole interaction between the substrate and the quadrupolar hydrogen molecule is attractive and is longer ranged than the dispersive forces. By controlling the charge of the sorbent, as in the case of capacitors, hydrogen could be encouraged to adsorb or desorb, as and when required. An increase of about 30% in the amount of hydrogen adsorbed on charged SWNTs compared with uncharged SWNT sorbents has been observed for realistic chemical charges of 0.1 e atom^{-1} [58].

The activation energies of the adsorption (E_a^{ads}) and desorption (E_a^{des}) processes play an important role in system kinetics. There is no barrier to be overcome in the adsorption process, i.e. $E_a^{ads} = 0$. But there is a significant barrier for the desorption process. To a first approximation, the magnitudes of the energy of adsorption and the activation energy for desorption are equal; $E_a^{des} \approx \Delta E$ (ads).

The adsorption energy of different hydrogen storage materials is shown in Fig. 12.

The favorable binding energy is in the region of 10–50 kJ mol^{-1}, because these values are acceptable for room temperature storage. Such values could be reached by carbon materials with:

(i) *Enhanced physisorption*: An enhanced physisorption takes place if the interlayer distance between graphene layers is optimized by spacers.

The additives act not only geometrically but also via a strong interaction with hydrogen. This interaction can increase the adsorption energy leading to a higher desorption temperature. However, this advantage must be weighed against the increase of the material density.

(ii) '*Kubas*' *binding*: Kubas [60] discovered molecular hydrogen complexes of transition metals. In these complexes, mostly organometal complexes, the chemical bond in the hydrogen molecule interacts with metals and leads to a relatively strong adsorption of molecular hydrogen. This interaction is due to donation of charge from the highest

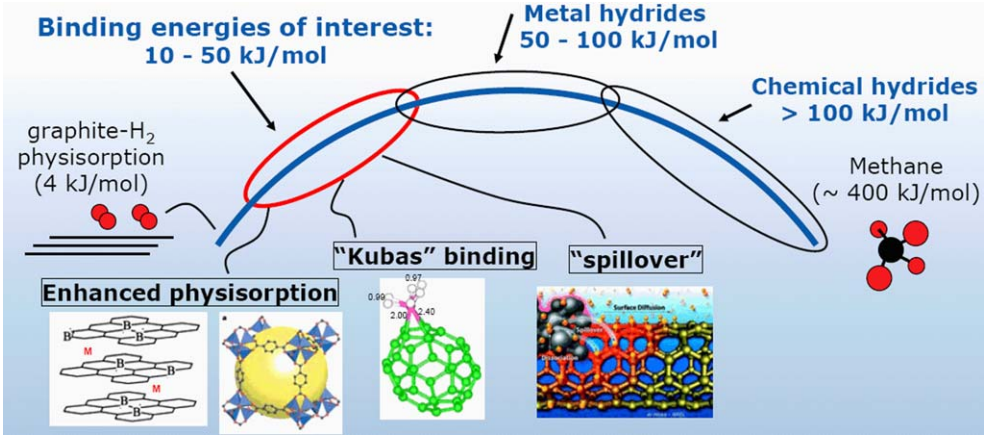

Fig. 12. Overview of the binding energies of different hydrogen adsorption materials [59].

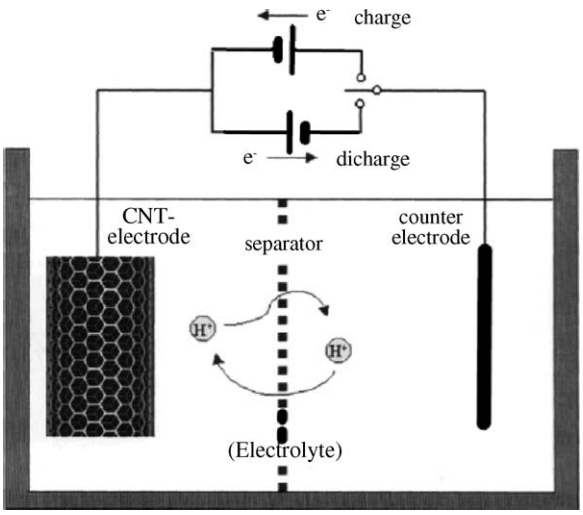

Fig. 13. Arrangement for electrochemical charging and discharging of hydrogen at a carbon nanotube [126].

occupied orbital of the ligand (H_2) to the empty metal orbitals and a subsequent back-donation from filled d-orbitals into the lowest unoccupied orbital of the ligand.

(iii) '*Spillover*': Additives act as a catalytic active center for the dissociation of hydrogen. The dissociated hydrogen atom then can *spillover* from the additive sites to the carbon network and finally become bound to carbon atoms.

This has been described, e.g. by Chen et al. for Li-doped MWNT [61].

3.4. "Electrochemical" adsorption

Normally the hydrogen is loaded into the carbon samples at high hydrogen gas pressure and low or ambient temperatures. An electrochemical method is also possible, in which the hydrogen storage unit is loaded and discharged via a counter electrode (see Fig. 13).

This could perhaps be a method of avoiding the need for cryogenic temperatures, as shown in Fig. 8. In that figure a hydrogen capacity–BET surface-line fits both samples which are gas-loaded at 77 K and samples that are electrochemically loaded at 298 K. In other words, an ambient temperature electrochemical charge could provide the same hydrogen storage results as a low temperature gas charge.

This electrochemical method, however, does not involve any special kind of adsorption. It is only a special method of inserting hydrogen. The hydrogen is formed in situ, i.e. directly at the storage site, avoiding transport processes. Because the charge reaction proceeds normally via an adsorbed atom (H_{ad}) the hydrogen could also be built into the carbon materials, atomically—without the need to overcome the dissociation barrier.

An overview of reported electrochemical methods has been published by Lipka [62].

4. Practical adsorption storage of hydrogen with carbon materials

4.1. Activated carbon

Activated carbon has low cost and is available on an industrial level. Therefore, it is an attractive option for the hydrogen storage application and consequently the interaction between hydrogen and this material have been extensively studied [63–65].

The hydrogen storage capability of activated carbon depends on the microstructure of the material, as mentioned in Section 3.1.

The storage mechanism is physisorption and the adsorption normally follows the Langmuir adsorption isotherm. This is shown in Fig. 14, where it is seen that only in the low pressure region are there divergences. Even at a hydrogen pressure of 15 MPa no saturation of the surface coverage is reached. No hysteresis between adsorption and desorption is observed.

At room temperature and moderate pressure only small quantities of stored hydrogen were found.

Although the hydrogen is mainly adsorbed by physisorption, surface groups and other reactive sites can also be incorporated into the activated carbon in order to promote hydrogen sorption although such processes tend to operate mostly via chemisorption and are thus not a useful means of enhancing the reversible storage of hydrogen.

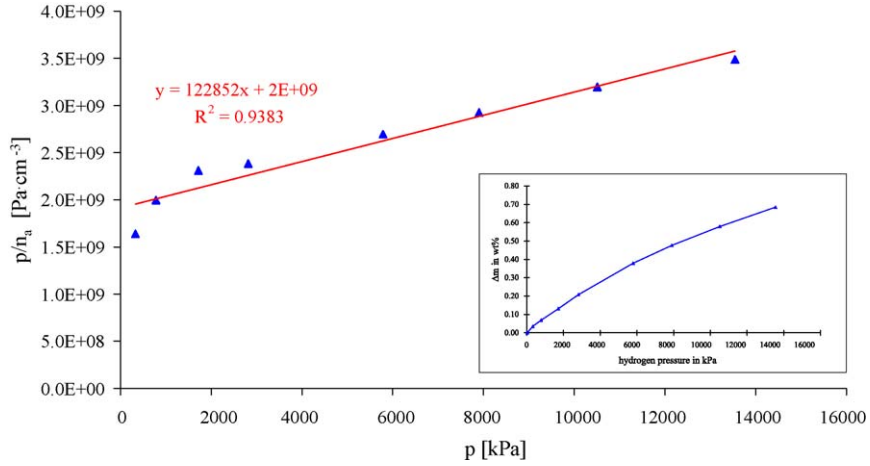

Fig. 14. Linearized Langmuir adsorption isotherm for an activated carbon sample ($S_{BET} = 2470\ m^2\ g^{-1}$) at 298 K.

Carbide derived carbons (CDC), with a specific surface of up to 2000 $m^2\ g^{-1}$ and up to 80% open pore volume, are promising class of materials for hydrogen storage. CDCs are produced by selective thermo-chemical etching of metal atoms from carbides (e.g. ZrC, TiC, SiC, and B_4C). At 77 K hydrogen storage capacities of CDCs at atmospheric pressures reached 3 wt% [66].

4.2. Graphite

Graphite is an inexpensive material that is available on an industrial scale. Although graphite has a relatively high polarizability, α_S, unfortunately its hydrogen storage capability is rather low [67], due to its small interlayer distances and its low specific surface area.

A surface area increase is achievable by ball milling [68]. After 4 h milling, the specific surface area can be as high as 700 $m^2\ g^{-1}$ as shown in Fig. 15.

It has been reported that after 80 h ball milling in a 1 MPa hydrogen atmosphere graphite nanostructures contain up to 0.95 H atoms per carbon atom, or 7.4 wt%, from which 80% could be desorbed at temperatures >600 K [46].

Intercalation of hydrogen into graphite at room temperature and moderate pressures should be possible by slightly expanding the interlayer spacing.

Many theoretical calculations have been carried out in attempts to understand the hydrogen adsorption process and to predict optimal graphite-like structures for hydrogen adsorption. This modeling has been based on empirical interaction calculations (e.g. [70–74]) and quantum mechanical calculations (e.g. [75–83]). The role of the quantum behavior of molecular hydrogen at low temperatures has been investigated, too [71,73,81–83]. Unfortunately none of these theoretical studies provides a reliable indication of whether or not the DOE target of 6.0% mass ratio could be achieved in pure graphitic materials.

Often in these calculations the binding capacity for hydrogen at near-ambient conditions, as well as the quantum effects and accurate ab initio-based interaction potentials, were not taken into account. A new calculation, which does take into account the contribution of quantum effects to the free energy and the equilibrium constant for hydrogen adsorption [84], shows that an optimized nanographite platelet (graphene) structure could store hydrogen at the level of the DOE target at room temperature and the moderate pressures of 10 MPa, provided that the graphite layer distance is spaced out between 6 and 7 Å. Practically this increase of the interlayer distance could be achieved by using well-defined spacers. Such spacers could have additional benefits such as acting as molecular sieves against N_2, CO, and CO_2, and they increase the mechanical stability of the nanographite.

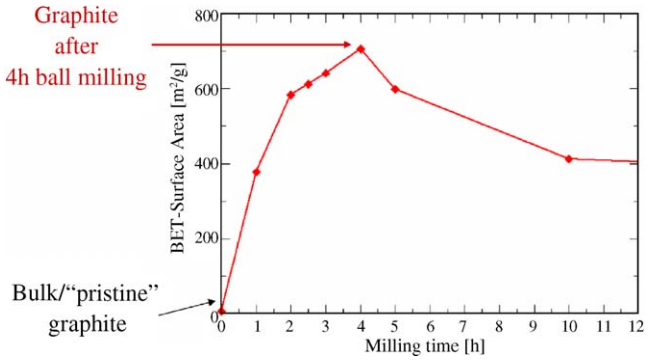

Fig. 15. BET surface of graphite vs. milling time [69].

Graphite intercalation compounds are well known to exhibit increased interlayer spacing [85]. For example, alkali metals or alkali bonded to organic ligands can be used and these expand the interlayer distance from about 3.4 to 8.7–12.4 Å [86,87]. Some intercalated metal ions are able to increase the hydrogen storage capacity at chemisorption sites [88]. It is important to note, however, that expansion of the spacing of the interlayer could lead to mechanical problems, such as exfoliation, at higher temperatures [89].

It is likely that the intercalation additives act not only by a geometric spacing effect but also via an electronic effect. It has been shown [90] that lithium dopants act as acidic cores to attract hydrogen molecules. The high electron affinity of the sp^2 carbon framework can separate the charge from the lithium, providing strong stabilization of the adsorbed molecular hydrogen.

Monte Carlo simulations with a first-principles derived force field model have elucidated this electronic effect at a pillared graphene sheet system with and without lithium doping (Fig. 16).

It was shown that, by optimization of the Li-pillared graphene sheet system, a hydrogen adsorption of up to 6.5 mass% at 2 MPa and room temperature should be possible [90]. Analogous calculations were made for Li-doped pillared single-wall nanotubes, and these suggested a hydrogen storage capacity of 6.0 mass% at 5 MPa and room temperature. Methods of synthesizing these Li-pillared systems were proposed.

Boron can also be added to graphite via some specially designed boron-containing precursor. Due to its similarity in atomic size and ability to form strong tricovalent bonds with adjacent carbons, the substitutional boron minimizes distortion

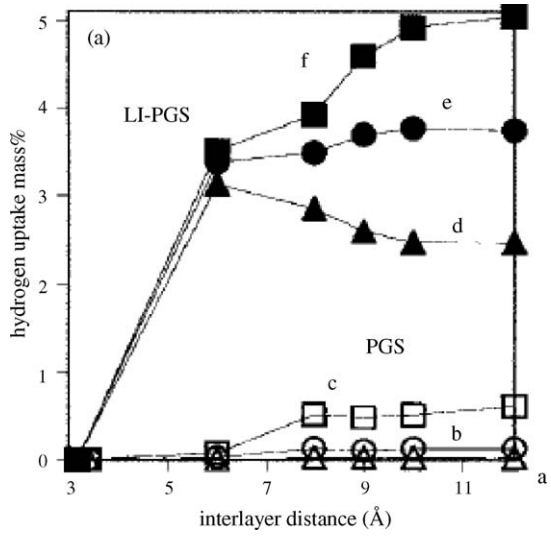

Fig. 16. Hydrogen storage capacities vs. interlayer distance of pillared graphene sheet systems—PGS (white) and Li-doped PGS (black) (Li:C = 1:6). Square (f and c): 5 MPa; circle (e and b): 1 MPa; triangle (d and a): 100 kPa [90].

of the lattice and preserves the graphitic structure. A slight expansion of the structure, caused by a lower van der Waals interaction, is possible as well.

4.3. Carbon nanostructures

4.3.1. Fullerenes

4.3.1.1. Buckyballs. C_{60} buckyballs show no hydrogen storage capability. This is in agreement with theoretical calculations showing only a very narrow window of collision energies for the formation of endohedral HC_{60} complexes [91].

First-principle calculations, however, have shown that a decoration of C_{60} and other buckyballs with transition metal atoms leads to an extensive hydrogen storage, where the nature of the hydrogen bonding is explained via Kubas interaction and the Dewar–Chatt–Duncason model [92].

The Dillon and Heben group [93] based its calculations on C_{60} and $C_{48}B_{12}$ samples. They indicate that charge transfer interactions should allow the formation of stable organometallic buckyballs with transition metals (e.g. Sc). A scandium atom can then bind as many as 11 hydrogen atoms, 10 of which are in the form of dihydrogen (binding energy 0.3 eV), that can be adsorbed and desorbed reversibly. The theoretical maximum retrievable hydrogen storage density of this system is ~9 wt%.

Independent reports of about 8 wt% hydrogen storage capacity were received from Yildirim et al. [94] with titanium and scandium each binding four hydrogen molecules (binding energy of 0.3–0.5 eV). Heavier metal such as manganese, iron, and cobalt do not bond onto C_{60}.

The Dillon and Heben group [95] also investigated possible sites for the metal additives in the buckyball via a Vienna Ab-initio Simulation Package (VASP) calculation. They assumed a simple model of a fullerene molecule with an iron attached (the iron itself having no practical value for hydrogen storage) with two different iron sites:

(A) The first iron atom was substitutionally included in the structure of a C_{36} fullerene.
(B) The second iron atom was bonded onto one of the carbon atoms of a C_{36} fullerene molecule.

In the first case the iron has no influence on the ability of nearby carbon atoms to bind hydrogen. But the iron species itself could bind up to three elongated hydrogen molecules to form $C_{36}Fe(H_2)_3$ via a back-donation of electrons in a manner similar to that seen for Kubas-type systems [96]. In this "enhanced physisorption" the hydrogen is non-dissociatively bound to the iron atom with an energy of 43 kJ mol^{-1}. This value is in good agreement with temperature profiled desorption measurements for iron-tipped multi-walled nanotubes.

In the second calculation it was found that a first hydrogen molecule can be bound only to the iron site. The H–H bond length is stretched from 0.74 to ~0.9 Å. Subsequent hydrogen molecules dissociate and break iron–carbon bonds and can also bind to neighboring carbon atoms in a kind of 'hydrogen spillover'.

The Komatsu group from the Kyoto University [97] has included hydrogen inside the buckyball, by a so-called molecular surgical method. They synthesized buckyballs with each ball perforated by a hole with a sulfur atom in its rim. Once the hydrogen molecule entered the hole, the buckyball was sewed up using a series of chemical reactions. Finally, the buckyballs were heated at 340 °C for 2 h to seal the gap. The process fills all the buckyballs with hydrogen, whereas alternative processes have yields of only a few percent.

4.3.1.2. Carbon nanotubes. After the discovery of nanotubes in 1993 attempts were soon made to use these materials for hydrogen storage [43,61,98–100]. Both single-wall nanotubes and multi-wall nanotubes were investigated.

An overview of experimental data on hydrogen adsorption in carbon nanotubes is given in the literature by Ding et al. [101].

Additionally it was found that multi-walled nanotubes can have a hydrogen storage capacity at room temperature of 1.97 wt% H_2 at 4 MPa [122], 3.7 wt% H_2 at 6.9 MPa [123], 4 wt% H_2 at 10 MPa [124], and 6.3 wt% H_2 at 14.8 MPa [125].

Table 2 shows hydrogen storage values between 0.05 and 21 wt%. The high values, however, have not so far been verified independently.

The storage values are dependent on many parameters of the carbon nanotubes, including their structure, structure defects, pretreatment, purification, geometry (surface area, tube diameter, and length), arrangement of tubes in bundles and/or 'ropes', storage pressure, temperature, etc. Rzepka et al. [35] studied these parameters in a grand factorial Monte Carlo program.

Hydrogen uptake varies linearly with tube diameter even though the tube volume increases as the square of the radius. This is because the uptake is proportional to the surface area (one layer adsorption), i.e. the number of carbon atoms, which increases linearly with increasing tube diameter. This is shown in Fig. 20 for the single-walled nanotube ($N_s = 1$).

The tube diameter can be controlled via the synthesis conditions. For example, an increase of the diameter of a single-walled nanotube to 1.85 nm by means of an arc discharge with a sulfur promoter (FeS) leads to a storage capacity of 4.5 wt%, where, however, only 3.3 wt% could be released under ambient pressure and room temperature. The residual stored hydrogen (1.2%) could be removed only by heating [99].

No complete agreement exists about the adsorption sites in carbon nanotubes. Theoretically the following sites exist:

- inside the tube;
- outside the tube;
- between tubes in 'bundles' and 'ropes';
- between the shells in multi-walled nanotubes.

For carbon nanotube bundles the adsorption sites are shown schematically in Fig. 17.

For hydrogen storage within the tube the hydrogen either must pass through the CNT wall or the tube must be open.

Normally as-formed tubes are closed at the tips by fullerene-like hemispherical structures. The tubes can then be opened by

Table 2
Summary of the reports of gaseous hydrogen storage capacity in carbon nanotubes

Sample	Purity (%)	T (K)	P (MPa)	H_2 (wt%)	Ref.
SWNT	Assumed 100	133	0.04	5–10	Dillon et al. [43]
SWNT	High	Ambient	0.067	3.5–4.5	Dillon et al. [102]
SWNT	∼50	300	10.1	4.2	Liu et al. [99]
Aligned SWNT	Purified	Ambient	11	4	Liu et al. [103]
SWNT	Purified	77–300	8	1–15	Chen et al. [104]
SWNT	High	80	∼7	8.25	Ye et al. [98]
MWNT	Purified	∼300–700	Ambient	0.25	Wu et al. [105]
SWNT	Purified	Ambient	4.8	1.2	Smith et al. [106]
SWNT-$TiAl_{0.1}V_{0.04}$	Sonicated >98	Ambient	0.067	6	Dillon et al. [107]
SWNT-Ti–6Al–4V	Purified	Ambient	0.08	1.7	Hirscher et al. [108]
SWNT-Fe	Purified	Ambient	0.08	<0.005	Hirscher et al. [108]
Ball-milled SWNT in Ar	<50	Ambient	0.08	<0.1	Hirscher et al. [109]
Ball-milled SWNT in D_2	<50	Ambient	0.9	0	Hirscher et al. [109]
CNT	Purified	298–773	0.1	0	Hirscher et al. [109]
Doped CNT	–	–	–	0.5–1.0	Zidan and Rao [110]
Li-CNT	Purified	473–673	0.1	20	Chen et al. [61]
K-CNT	Purified	<313	0.1	14	Chen et al. [61]
Li-CNT (wet H_2)	Purified	473–673	0.1	12	Yang [111]
Li-CNT (dry H_2)	Purified	473–673	0.1	2.5	Yang [111]
K-CNT (wet H_2)	Purified	<313	0.1	21	Yang [111]
K-CNT (dry H_2)	Purified	<313	0.1	1.8	Yang [111]
Li-CNT	10–40	473–663	0.1	0.7–4.2	Pinkerton et al. [30]
SWNT	80–90	273	0.04	7	Dillon et al. [107]
SWNT	90 vol%	298	–	0.63	Ritschel et al. [112]
MWNT	Unpurified	298	–	0.5	Ritschel et al. [112]
MWNT	Unpurified	293	6.5	2	Ding et al. [113]
CNT	–	Ambient	Ambient	0.5	Adu et al. [114]
SWNT	Purified	77	0.2	6	Pradhan et al. [115]
Aligned MWNT	High	298	10	3	Zhu et al. [116]
Aligned MWNT	High	290	10	2.4	Cao et al. [117]
Random MWNT	High	298	10	0.68	Zhu et al. [116]
MWNT	High untreated	300	1.0	5–7	Chen et al. [118]
MWNT	High acid treated	300	1.0	13.8	Chen et al. [118]
MWNT	High	300	7.0	0.7–0.8	Badzian et al. [119]
SWNT	Unpurified	295	0.1	0.93	Nishimiya et al. [120]
SWNT	Unpurified	77	0.1	2.37	Nishimiya et al. [120]
MER MWNT	10–15%	298	3.6	0.03	Tibbetts et al. [121]
Rice SWNT	High	298	3.6	0.05	Tibbetts et al. [121]
CNT	–	298	11.35	11.26	Chambers et al. [3]

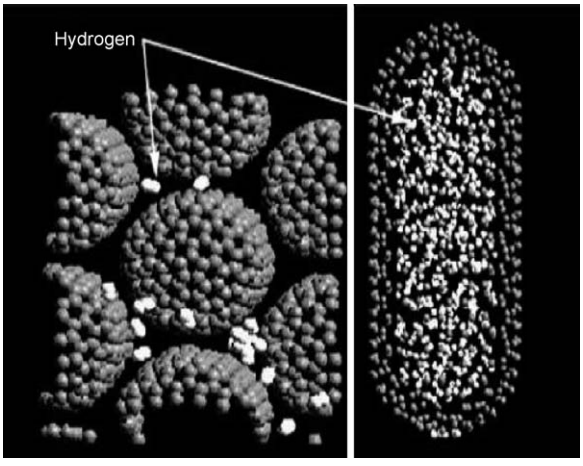

Fig. 17. Potential sites for hydrogen adsorption within a nanotube bundle; (left) interstitial sites between tubes and (right) inside the tube [1].

chemical (e.g. HNO_3) or ultrasound treatment. Because Dillon et al. [102] found a strong increase in hydrogen uptake after an oxidative opening of the tubes, they concluded that most of hydrogen is stored inside the tubes.

Calculations carried out by Seifert and Lee et al. [126,127] show that the transport of hydrogen through the carbon tubes is strongly suppressed by a steric barrier. This barrier can be overcome by an electrochemically assisted 'knock-on' process (Fig. 18).

For closed tubes, therefore, the adsorption can take place only on external surfaces of carbon nanotubes or in interstitial spaces between single nanotubes. Normally the products of the synthesis of single-walled nanotubes are 'bundles' and 'ropes'. The generation of ropes is based on a strong cohesive interaction between the tubes. The distances between the tubes in the ropes are too small for an extensive intercalation of hydrogen into the ropes. Therefore, hydrogen is adsorbed only on the outer surface of ropes. Intercalants into the ropes could separate the single nanotubes and increase the adsorption area [128]. A delamina-

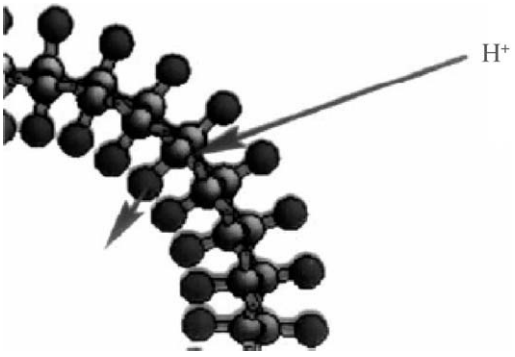

Fig. 18. 'Knock-on' of an interior bound hydrogen in a zigzag H-carbon nanotube by a proton approaching from the outside [126].

tion of the ropes and bundles, respectively, would also enhance the available adsorption surface.

The Dillon and Heben group [102] assumed the existence of special cavities in the carbon nanotube bundles with a high activation energy of desorption (which is approximately similar to the adsorption energy; see Section 3.3). This hypothesis is based on the thermal desorption curves of different single-walled nanotube samples. A laser-generated, and purified, open single-walled nanotube sample, which was 'charged' with hydrogen at 30 kPa by cooling down from 273 to 70 K shows a 'high-temperature desorption' at temperatures >300 K (see Fig. 19).

Also, the inter-shell distances of a multi-walled nanotube are too small for effective hydrogen adsorption. Most of the shells are inactive for hydrogen adsorption and only serve to increase the carbon mass and therefore to decrease the hydrogen storage capacity, as calculated by Züttel et al. [129] and shown in Fig. 20.

A dissociative adsorption (chemisorption) of hydrogen can also take place on carbon nanotubes. At a single single-walled

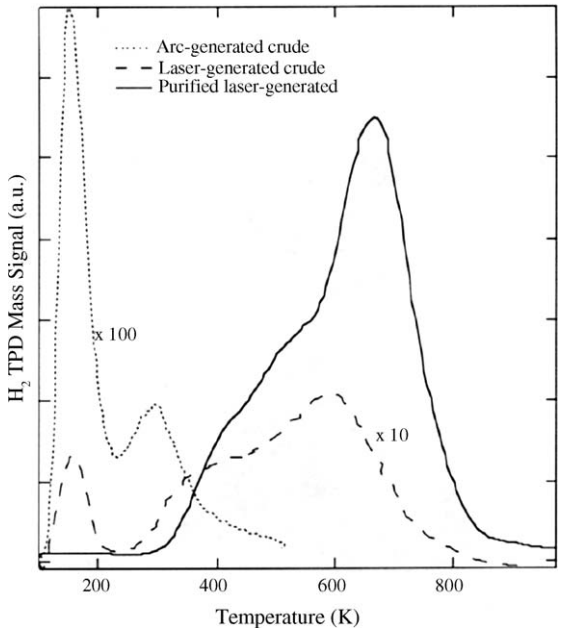

Fig. 19. Thermal desorption curves of different generated and purified single-walled nanotubes, after hydrogen charging at 30 kPa and cooling down from 273 to 70 K [102].

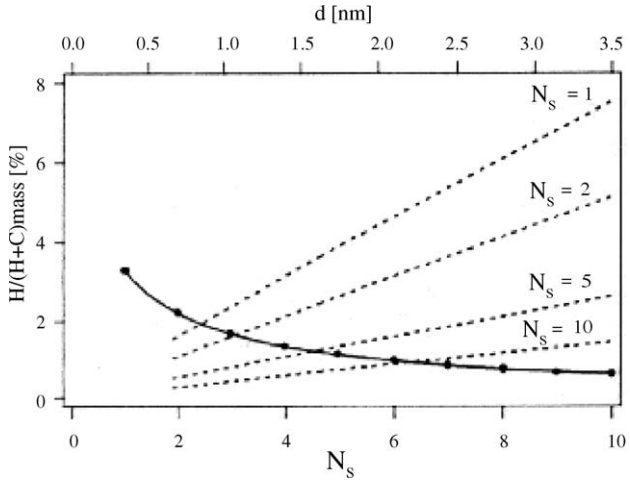

Fig. 20. Calculated hydrogen storage density (mass%) of multi-walled nanotubes:
- vs. numbers of shells N_s (continuous line);
- vs. tube diameter d (dotted line) for nanotubes with different shell numbers (N_s) ($N_s = 1$ means a single-walled nanotube) [129].

nanotube this is difficult, due to the van der Waals repulsion. In a carbon nanotube bundle, however, chemisorption should be possible, because the van der Waals repulsion is reduced, especially at high pressure as this reduces the C–C distance between two adjacent carbon nanotubes from 3.8 to 2.6 Å—a value which is ideal for capturing hydrogen in a dissociative process [130].

It is well known that increasing hydrogen pressure leads to a higher hydrogen capacity. Pressure (and temperature), however, also exercises an influence on the mechanical behavior of carbon nanostructures. Ye et al. [98] have observed a phase transition of single-walled nanotubes at 77 K, which indicates a separation of the tubes. Furthermore it was reported that excessive hydrogen adsorption leads to a breakdown of the tube structure, caused by large repulsive energies [131]. Similar effects were observed with graphite nanofibers by the Rodriguez group [132]. They found an expansion of the spacing between the graphite layers as a result of high hydrogen pressure (Fig. 21).

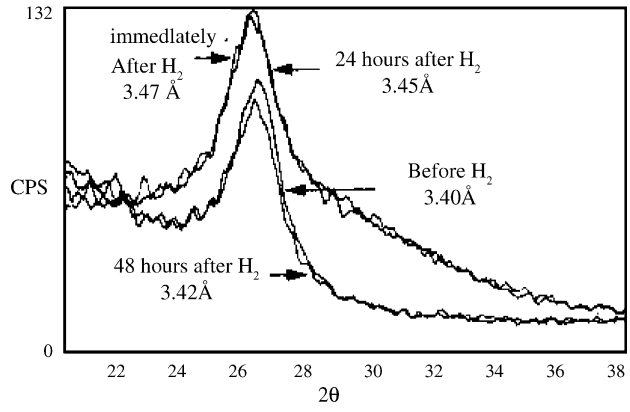

Fig. 21. Plots of the 0 0 2 X-ray diffraction peak of carbon nanofibers before hydrogen adsorption, immediately after hydrogen adsorption at an initial pressure of 11.2 MPa, and 24 and 48 h after desorption [132].

The adsorption under high hydrogen pressure leads to an expansion of the lattice spacing from 3.40 to 3.47 Å. This spacing remains high (3.45 Å) 24 h after the desorption of the hydrogen. Only 48 h after the desorption did the spacing return to a value (3.42 Å) close to that before the high pressure adsorption.

4.3.1.3. Additives to carbon nanostructures. Because the targets set by the DOE have not been achieved reproducibly, attempts have been made to use additives to carbon materials in order to increase the hydrogen storage capacity. These additives have three effects:

- introducing structural changes, e.g., expanding interlayer distances;
- changing the electronic structure of the carbon sample;
- acting as a distinct hydrogen storage material (creating a hybrid material).

It is not easy to separate these effects as they can occur simultaneously.

4.3.1.3.1. Crystal structure changes. The intercalation of alkali metals into graphite was extensively examined during the 1970s. Alkali metal intercalation causes the spacing between the graphitic layers to be increased and therefore facilitates hydrogen diffusion into the material. Chen et al. [61] have doped multi-walled nanotubes with lithium and potassium. The potassium-doped MWNT can adsorb hydrogen even at ambient temperature, but is chemically unstable. Chemically stable lithium-doped MWNTs can store and desorb hydrogen at elevated temperatures (473–673 K). The amounts of hydrogen reported to have been stored, 20 wt% for Li-MWNT and 14 wt% for K-MWNT, have not, however, been validated (see Section 4.5).

Ahn et al. [128] carried out a neutron powder diffraction study to investigate the structures of such carbon intercalations, e.g. KC_{24} (see Fig. 22), and their ability to adsorb hydrogen (as its deuterium isotope).

4.3.1.3.2. Electronic structure changes. As already mentioned in Section 4.2 lithium dopants can act as (acidic) cores to attract hydrogen molecules. The high electron affinity of the sp^2 carbon framework tends to separate the charge from the Li, providing strong stabilization of the molecular hydrogen. Calculations have indicated that this should be possible not only for graphite but also for lithium-doped pillared single-walled nanotubes (6 wt% of hydrogen stored at room temperature and 5 MPa) [90].

A recent first-principles study [133] demonstrated that a single titanium atom coated on a single-walled nanotube should bind up to four hydrogen molecules, leading to 8 wt% of hydrogen storage. It was concluded that the interactions between the carbon, titanium, and hydrogen change the carbon electronic structure and seem to give rise to unusual attractive forces. These forces are expected to be based on Kubas binding [60].

4.3.1.3.3. Hybrid materials. When carbon nanotubes are used in combination with other hydrogen storage materials there is a synergetic effect in addition to the contribution of the hydrogen storage values of the individual materials. This effect is based on changes of both the crystal structure and the electronic structure.

Titanium and titanium alloys are both hydrogen storage materials. It has been reported [94] that such materials, in combination with single-walled nanotubes, have a hydrogen uptake of 2–8 wt%. Fig. 23 shows a hydrogen storage capacity for a Ti–Al–V alloy in combination with SWNT of about 3 wt% at room temperature and 80 kPa.

This diagram shows that alloyed single-walled nanotubes exhibit an increase in hydrogen uptake as compared with the alloy alone. Measurements of the alloy alone have consistently yielded 2.5 wt% (represented by the dark thick line in the graph) of hydrogen uptake.

Hirscher et al. [108] and Guay et al. [134] have also investigated titanium additives. They came to the conclusion that this route will not allow the DOE targets to be met.

$NaAlH_4$, a chemical hydride, is another well known material with a reversible hydrogen storage capability (∼5.5 wt%),

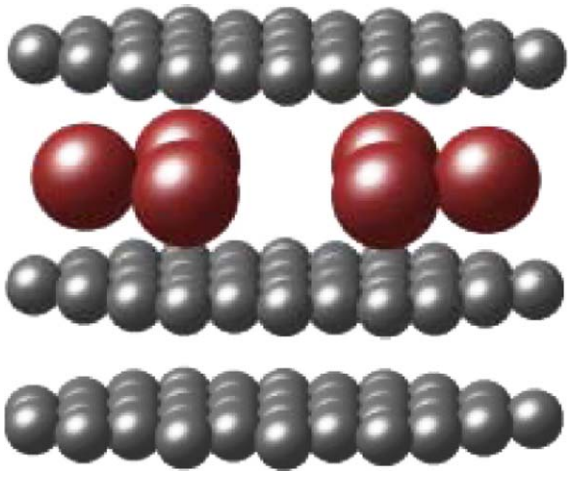

Fig. 22. Stacking sequence of KC_{24}; small atoms: carbon; large atoms: potassium atoms.

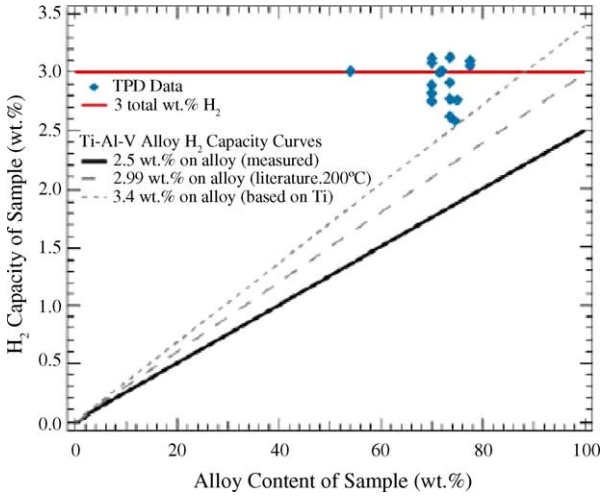

Fig. 23. Hydrogen storage capacity of single-walled nanotube-metal alloy samples (rhombus points), and metal alloys (linear rising lines) [95].

Table 3
Summary of reported hydrogen gas storage capacity in carbon nanofibers

Sample	Purity (%)	T (K)	P (MPa)	H_2 (wt%)	Ref.
GNF herringbone	–	298	11.35	67.55	Chambers et al. [3]
GNF platelet	–	298	11.35	53.68	Chambers et al. [3]
GNF	–	77–300	0.8–1.8	0.08	Ahn et al. [137]
CNF	–	300	12	6.5	Browning et al. [138]
GNF	–	300	10.5	0.7	Poirier et al. [139]
CNF	–	293	10	1	de la Casa-Lillo et al. [140]
CNF	–	298	12	1.4	Hwang et al. [141]
Ball milled GNF	–	Ambient	0.9	0.5	Hirscher et al. [109]
GNF	–	300	11	<0.1	Hirscher and Becher [142]
Vapor grown carbon fibers	–	298	3.6	<0.1	Tibbetts et al. [121]
CNF	–	300	12.5	1.6	Ströbel et al. [143]
GNF herringbone	Purified	77–300	1.5	1–1.8	Ströbel et al. [143]
GNF	–	300	12	10	Gupta and Srivastava [144]
GNF	–	300	12	10	Gupta and Srivastava [145]
CNF	–	77	12	12.38	Fan et al. [146]
CNF	–	300	11	5.7	Cheng et al. [147]

but it has unfavorable kinetics [135]. When ball-milled with single-walled nanotubes, a Zr/Ti-doped $NaAlH_4$-SWNT system exhibits sorption kinetics enhanced by a factor of 4 at 160 °C and for up to 200 sorption (2.3 MPa)–desorption (25 kPa) cycles [136]. After 200 cycles the composite lost some of its storage capacity. A similar effect, but to a lesser extent, was found for graphite and activated carbon additives.

The results found indicate that, by creating new hydrogen transition sites, the structure of carbon in the composites plays an important role in enhancing the hydrogen absorption and release rates by facilitating hydrogen diffusion and thermal energy transfer.

4.3.2. Carbon nanofibers

An overview of experimental data on hydrogen adsorption in carbon nanotubes published in the literature has been given by Ding et al. [101].

Table 3 shows hydrogen storage values between 0.1 and 67.55 wt%.

Extraordinary hydrogen storage values were found by the group of Rodriguez and Baker [3,148,149]. They measured up to 67 wt% of hydrogen with herringbone structured graphite nanofibers, and up to 54 wt% of hydrogen with platelet structures at 278 K and about 12 MPa. It was suggested that the GNF values are caused by expanding the spacing between the graphite layers (see Fig. 24) as a result of the high hydrogen pressure and water vapor [132]. A semi-quantitative scheme for the adsorption has been given by Baker [21].

Relatively high adsorption values, in the range of 4–7 wt%, of hydrogen on herringbone graphite nanofibers were reported by the British Defense Evaluation & Research Agency and Loughborough University [150]. Gupta and Srivastava [144,145] found 10 wt% of hydrogen and Fan et al. [146] about 12 wt%.

None of these high values has been reproduced in other laboratories (see also Section 4.5).

Our own measurements [143,152] have shown adsorption values at herringbone graphite nanofibers below 1 wt%. It is interesting to note that the adsorption/desorption isotherms for all investigated GNF samples have shown a strong hysteresis (see Fig. 25).

Maybe this hysteresis effect is the consequence of a reversible structural change caused by the hydrogen pressure, as discussed by Rodriguez [148].

The hydrogen storage capacities are strongly influenced, not only by the synthesis and purification conditions, but also by the pretreatment of the graphite nanofibers [151,153]. The pretreatment creates edge dislocations and causes a spreading of adjacent layers in the crystal structure and these features can become regions for preferential adsorption of hydrogen.

Attempts to increase the hydrogen uptake by graphite nanofibers have followed similar lines to those used in the case of carbon nanotubes. Composites of metal hydrides ($LaNi_5$ and $TiAl_{0.12}V_{0.04}$) with graphite nanofibers, or even Pd [154], have been used. Graphite nanofibers can be purified by removing amorphous carbon, and caps over the graphite layers can be removed to open up more planes for hydrogen adsorption.

Further improvements can be sought for graphite nanofibers by carbon exfoliation via intercalation of high concentration acids followed by thermal shock, which leads to a strong increase of the surface area.

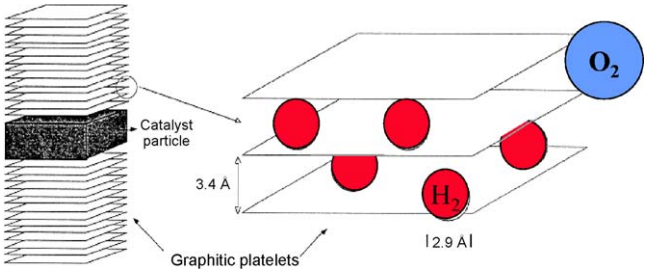

Fig. 24. Scheme of hydrogen adsorption at platelet graphite nanofibers.

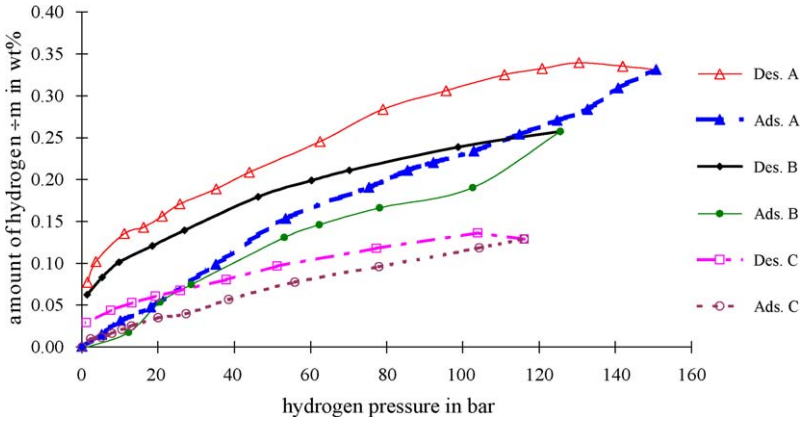

Fig. 25. Adsorption (Ads) and desorption (Des) isotherms (298 K) of different graphite nanofibers synthesized via catalytic chemical vapor deposition ((A) 192 $m^2\ g^{-1}$, (B) 168 $m^2\ g^{-1}$, and (C) 508 $m^2\ g^{-1}$).

4.4. Electrochemical storage of hydrogen in carbon materials

A summary of reported electrochemical hydrogen storage in carbon materials is given by Lipka [62] (see Table 4).

Table 4 shows electrochemical hydrogen storage values between 0.27 wt% and about 2.9 wt%, with the exception of the 6.1 wt% value of Liu, which, to date, has not been reproduced by other groups. In other words, the electrochemical storage of hydrogen leads to approximately the same hydrogen capacities as the gas storage method.

The addition of dopants or extra conductive materials to the nanocarbon electrode is important because the C–H bond formation changes the electronic properties of carbon nanotubes from metallic to semiconducting [169]. The most commonly used additives are metals such as gold, nickel, copper, or palladium all in the form of micrometer-sized powders or as nanosized particles decorating the carbon surface.

The electrodes are prepared by mixing and grinding of carbon particles with metals (to increase conductivity) and organic binders. This mixture is then pressed to form an electrode. The electrode is cathodically charged with hydrogen. The hydrogen release takes place anodically. The coulomb efficiency is about 60%.

From the literature it is not clear whether the hydrogen is stored as molecules or as atoms. Because the storage capacity is relatively strongly increased in the presence of metals it is assumed that the metal acts also as a catalyst, which promotes the formation of H_{ad} via a spillover (from the metal to the carbon surface):

$$H_2O + e^- + M \Rightarrow M^{\bullet}H_{ad} + OH^- \quad (3)$$

$$M^{\bullet}H_{ad} + C \Rightarrow C^{\bullet}H_{ad} + M \quad (4)$$

The storage capacity is influenced not only by the catalyst but also by the electrolyte, the carbon material, the charge and discharge conditions, and – this is especially interesting – the atmosphere. If the charging of the electrode takes place in the presence of pressurized hydrogen more hydrogen is stored than is the case for charging in ambient air.

It seems that in constant experimental conditions, the effective surface of the carbon material determines the storage capacity (as indicated in Fig. 8).

Table 4
Summary of reported electrochemical hydrogen storage in carbon materials

Material	Experimental conditions	H_2 (wt%)	Ref.
SWNT-Pd powder (1:4)	6 M KOH, room temperature, 1 atm, I_{disch} = 2.5–5 A g^{-1}	0.39	Nutzenadel et al. [155]
Activated carbon (1200–1500 $m^2\ g^{-1}$)	6 M KOH, room temperature, 1 atm, I_{disch} = 100 mA g^{-1}	1.5	Jurewicz et al. [156]
MWNT/Ni (1:10)	6 M KOH, room temperature, 1 atm, I_{disch} = 200–1000 mA g^{-1}	0.7	Qin et al. [157]
CNT/Ni powder (4:5)	6 M KOH, room temperature, 1 atm, I_{disch} = 0.4 mA g^{-1}	0.34	Lee et al. [158]
SWNT/Cu (1:3)	30% KOH, room temperature, 1 atm, I_{disch} = 10–100 mA g^{-1}	2.9	Rajalakshmi et al. [159]
HNO_3 treated CNF/Ni	6 M KOH, room temperature, 1 atm, I_{disch} = 100 mA g^{-1}	0.27	Youn et al. [160]
SWNT/Ni powder (1:3)	6 M KOH, room temperature, 1 atm, I_{disch} = 400 mA g^{-1}	1.2	Dai et al. [161]
CNT/Ni–P particles + Ni powder (1:3)	6 N KOH, room temperature, 1 atm, I_{disch} = 1000 mA g^{-1}	1.1	Gao et al. [162]
CNF/Ni–P particles (<76)	6 M KOH, room temperature, 1 atm, I_{disch} = 1000 mA g^{-1}	0.30	Yan et al. [163]
MWNT (electrochem.)	18 M H_2SO_4, 20 °C, 1 atm, cyclic voltammetry	1.61	Skowronski et al. [164]
CNT/Ni powder (1:20) CNF/Ni powder (1:20)	6 N KOH, room temperature, 1 atm, I_{disch} = 800 mA g^{-1}	1.0, 0.25	Chen et al. [165]
MWNT/Cu particles	6 M KOH, room temperature, 1 atm, I_{disch} = 1500	6.1	Liu et al. [166]
SWNT pressed into Ni foam	6 M KOH, room temperature, 1 atm, I_{disch} = 25 mA g^{-1}	1.84	Dai et al. [167]
Electrochem. Ox. MWNT in HNO_3	6 M KOH and 0.3 M H_2SO_4, CV and I_{disch} = 20 mA g^{-1}	0.3	Lombardi et al. [168]

4.5. Unexpected hydrogen storage

As shown in both Tables 2 and 3 extremely high hydrogen storage values (up to 67.55 wt% for the herringbone GNF structure) have been reported.

As already mentioned a worldwide effort to verify these large hydrogen storage values in various nanostructured carbons, however, has not been successful. It is surprising, therefore, that very often these values continue to be cited in the literature without any acknowledgement of their uncertainty.

The reasons why confirmation of these results has not been forthcoming could include the following:

- *Low purity of samples*: Syntheses of carbon nanostructured samples, especially those formed shortly after the discovery of these structures, tended to produce rather impure phases. Very often only small fractions of carbon nanotubes or carbon nanofibers were found in the products and the hydrogen storage capacity of those samples was extrapolated in order to predict the capacity of pure materials.

  For example, a storage capacity of about 10 wt% was reported [102] for open single-walled nanotubes. This high value, however, is an extrapolation from a sample with only 0.05% of nanotubes to arrive at the value for a pure material. Later, with more concentrated samples, the extrapolation only reached values of 3.5–4 wt% at room temperature and 70 kPa.
- *Insufficient characterization of samples*: The carbon samples are very often a mixture of single-walled nanotubes, multi-walled nanotubes, and carbon nanofibers with various diameters, lengths, chiral vectors (in the case of nanotubes), shell numbers (in the case of multi-walled tubes), open and closed structures (tubes), etc. As a result of all this potential variability it would not be surprising to find a large range of hydrogen storage values.
- *Contamination of samples*: For example, a storage capacity of about 4.5 wt% of hydrogen was found [43] for single-walled nanotubes at 30 kPa and 70 K. Only a few milligrams of SWNTs were used for these investigations and the tubes were opened by a high power ultrasonic procedure in nitric acid. The ultrasonic horn that was used was made from a corrosion-resistant Ti–6Al–4V alloy. This alloy, however, is also a hydrogen storage material. Hirscher et al. [108] have shown that nearly all of the storage capacity of the sonicated samples examined in this work can be attributed to the hydrogen uptake of titanium alloy particles which have contaminated the carbon samples during sonication.
- *Hydrogen contamination*: Chen et al. [61] found hydrogen storage capacities up to 20 wt% for lithium-doped multi-walled nanotubes and up to 14 wt% for lithium-doped graphite. It was shown, however [30,152,170], that the majority of the weight changes in this case are caused by adsorbed water, which was present as a contaminant in the hydrogen. Furthermore the Li_2O used for the carbon treatment is both hygroscopic and able to adsorb carbon dioxide. Both of these processes lead to weight gains that could be mistakenly attributed to hydrogen uptake.
- *Technical problems*: The relatively complicated methods of synthesis of these materials often result in the production of only a rather small mass of carbon nanotubes and/or nanofibers. There is thus considerable scope for errors during gravimetric or volumetric measurement.

  In addition, inaccurate cooling of the hydrogen gas after pressurization can lead to effects that simulate adsorption.

  Problems can also arise through leaks in measurement equipment.

A good overview of experimental methods for hydrogen adsorption measurement problems and problems of interpretation of the results is given by Ding et al. [101].

The extremely high values of hydrogen uptake found by the group of Rodriguez and Baker (Chambers et al. [3]) have not been validated (e.g. [152]). The storage value of 67.55 wt% corresponds to about 24 hydrogen atoms for each carbon atom! Up to now no explanation has been put forward to account for this very unusual result. The group that produced the original report has now published a reduced value of a maximum of 3.8 wt% hydrogen storage at 6.5 MPa and room temperature [151] but with only general remarks about difficulties associated with the system.

5. Applications

The 2010 DOE technical targets for hydrogen storage systems for practical use on-board vehicles are given in Table 5 [171].

It is important to recognize the following points in relation to the set of technical targets.

5.1. High rate kinetics for charge and discharge

The storage capacity must be realized for both discharge and charge very rapidly. Therefore, the charge and discharge kinetics must be very high.

The kinetics are strongly influenced by the structure of the carbon materials. Materials with higher tube diameters and larger interlayer distances between the tubes and fibers are favored. For carbon nanotubes, for example, it has been shown, based on a theoretical calculation taking into consideration the Arrhenius law and the quantum Boltzmann kinetic equation, that

Table 5
DOE technical targets for hydrogen storage systems (for 2010)

Parameter (units)	Targets
Storage capacity (wt%)	6.0
Energy efficiency (%)	97
Energy density ($Wh\,l^{-1}$)	1100
Specific energy ($Wh\,kg^{-1}$)	2000
Cost ($US\$\,kW\,h^{-1}$)	5
Operating temperature (°C)	−40 to +50
Start-up time to full flow (s)	15
Hydrogen loss ($scc\,h^{-1}\,l^{-1}$)	1.0
Refueling time (min)	<5
Cycle life (cycles)	500
Recoverable usable amount (%)	90

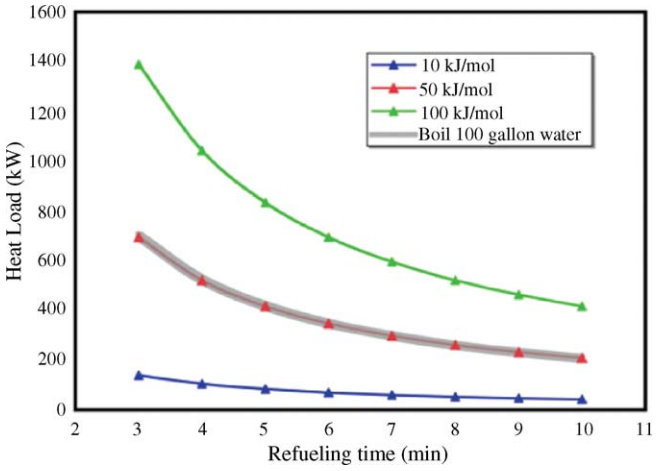

Fig. 26. Heat load vs. refueling time for 5 kg of hydrogen [174].

there exists a minimum diameter of the nanotubes which must be exceeded for the diffusion coefficient to remain large. This critical diameter for the diffusion of atomic hydrogen is about 5 Å [172].

Furthermore the adsorption energy exercises considerable influence on the design of the storage system. Fig. 26 shows the heat load that is generated during the charge of 5 kg of hydrogen. A high adsorption energy increases the heat load and therefore also the refueling time. Large heat exchangers are then necessary.

5.2. High efficiency of the charge–discharge cycle

The necessary energy for the charge and discharge process must be low. The charge energy is mostly pressure energy and the discharge energy mostly thermal energy, both of which must be provided externally, reducing the efficiency of the system. The heat for discharge (desorption), however, can come via the polymer electrolyte fuel cell waste heat on-board a vehicle. The thermal energy necessary depends on the hydrogen adsorption energy of the material used for the hydrogen storage. The heat energy–discharge time relationship is similar to the heat–refueling time relationship which is shown in Fig. 26.

5.3. Charge–discharge cycle stability

The carbon hydrogen storage system must have a high long-term stability, at least in the order of the lifetime of a car. There has been one report [173] of a proprietary carbon material which shows only a minor loss of about 5% in adsorptive capacity, after 3000 full cycles. There was no evidence of mechanical damage from cyclic swelling and the carbon does not appear to comminute (degrade to a fine powder), which has been a typical problem with other activated carbons.

5.4. Preferably work at ambient temperature and pressure

The DOE targets for operating temperature range are −40 to +50 °C. Cryogenic temperatures are not expected to be acceptable for economic reasons. Nevertheless, it has been shown, through a systems analysis [174], that the DOE target for 2005 (4.5 wt% H_2) could be met with an isolated aluminium container (see Fig. 27) and a commercially available activated carbon material (300 g m^{-2}) at a temperature of 77 K and a pressure of 5–10 MPa.

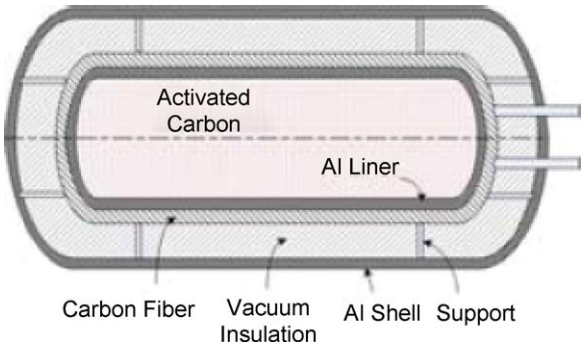

Fig. 27. Scheme for a low temperature carbon hydrogen storage system [174].

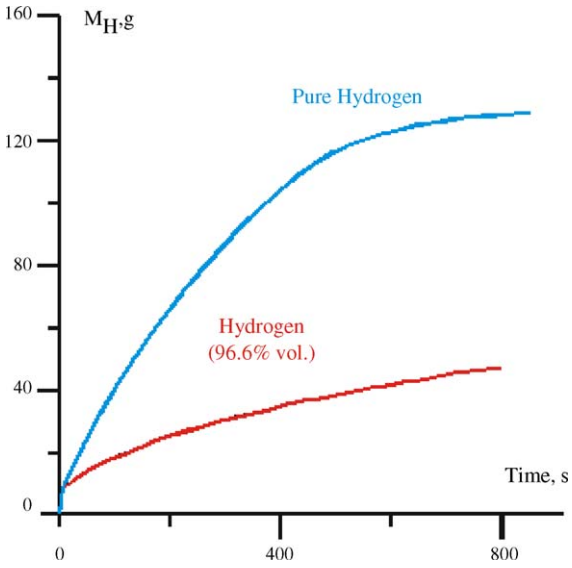

Fig. 28. Sorption of pure and impure hydrogen, results based on calculations [175].

5.5. Hydrogen purity

Non-adsorbable impurities dramatically decrease the efficiency of hydrogen adsorption systems, affecting kinetics, heat and mass transfer, refueling time, and energy conversion efficiency in fuel cells. Fig. 28 shows the influence of purity on the kinetics of adsorption.

6. Summary and outlook

The room temperature hydrogen storage capacities reported in the literature can be divided into three groups [176]:

- >14 wt% hydrogen storage, for which the reports are thought to be incorrect.

- 3–14 wt% hydrogen storage, for which the reports are thought to be not a priori incorrect, because theoretical calculations permit such values, but no reproducible verification exists.
- 0–3 wt% hydrogen storage are consistent with expectations based on experimental findings for high surface area carbons.

The, early, spectacular hydrogen storage capacities reported for nanostructured materials at near-ambient temperature have not been independently verified by other laboratories. Therefore, the initial euphoria is over and we now have a realistic view of the possibilities for the storage of hydrogen in carbon materials.

Practical hydrogen storage capacities <3 wt% have been found in a variety of nanostructured carbon materials. This is well short of the DOE 2010 target of 6.0 wt% and also short of the target for 2005 of 4.5 wt%.

Recent theoretical calculations, however, predict a possible hydrogen uptake of ≥6.0 wt% for carbon materials with a suitable structure. The following carbon structures are especially promising:

(i) *Nanostructured graphite with optimum interlayer spacing*: Calculation by a joint group of Ottawa and Dresden (Seifert) has shown that nanographite platelets with an interlayer spacing of about 8 Å are very promising. Instructions for a synthesis of nanostructured graphite via spacers are given [84].

(ii) *Organometallic decoration of buckyballs and single-walled nanotubes with transition metals*: the Dillon and Heben group [93] based its calculation on C_{60} and $C_{48}B_{12}$ samples with scandium as the transition metal and the Yildirim group [94,133] focused on C_{60} and SWNTs with titanium as the transition metal. In both cases the high hydrogen storage value expected depends on KUBAS binding.

The task for the future is now to synthesize the modeled carbon materials.

Acknowledgement

We like to thank Prof. Dr. K. Bohmhammel (TU Bergakademie Freiberg) for the excellent support in all experimental as well scientific questions.

References

[1] K. Atkinson, S. Roth, M. Hirscher, W. Grunwald, Fuel Cell Bull. 38 (2001) 9.
[2] A. Bouza, C.J. Read, S. Satyapal, J. Milliken, DOE Hydrogen Program, FY 2004 Program Review.
[3] A. Chambers, C. Park, R.T.K. Baker, N.M. Rodriguez, J. Phys. Chem. B 102 (1998) 4253.
[4] H. Marsh, F. Rodriguez-Reinoso, Activated Carbon, Elsevier, 2005.
[5] F. Rodríguez-Reinoso, Encyclopedia of Materials: Science and Technology, Elsevier, 2004, p. 22.
[6] K.S. Novoselov, A.K. Geim, S.V. Morozov, D. Jiang, Y. Zhang, S.V. Dubonos, I.V. Grigorieva, A.A. Firsov, Science 306 (2004) 666.
[7] H.W. Kroto, J.R. Heath, S.C. O'Brien, R.F. Curl, R.E. Smalley, Nature 318 (1985) 162.
[8] W. Krätschmer, L. Lamb, K. Fostiropoulos, D. Huffman, Nature 347 (1990) 354.
[9] A. Jorio, G. Dresselhaus, Encyclopedia of Physical Science and Technology, Elsevier, 2004, p. 315.
[10] S. Subramoney, Encyclopedia of Materials: Science and Technology, Elsevier, 2001, p. 941.
[11] S. Margadonna, K. Prassides, Encyclopedia of Materials: Science and Technology, Elsevier, 2001, p. 3379.
[12] S. Iijima, Nature 354 (1991) 56.
[13] S. Iijima, T. Ichihashi, Nature 363 (1993) 603.
[14] D.S. Bethune, C.H. Kiang, M.S. de Vries, G. Gorman, R. Savoy, J. Vazquez, R. Beyers, Nature 363 (1993) 605.
[15] M.S. Dresselhaus, G. Dresselhaus, R. Saito, Carbon 33 (1995) 883.
[16] D.S. Bethune, C.H. Kiang, M.S. de Vries, G. Gorman, R. Savoy, J. Vazques, R. Beyers, Nature 363 (1993) 605.
[17] C.E. Baddour, C. Briens, Int. J. Chem. Reactor Eng. 3 (2005) R3.
[18] K. Saïdane, M. Razafinimanana, H. Lange, A. Huczko, M. Baltas, A. Gleizes, J.L. Meunier, J. Phys. D: Appl. Phys. 37 (2004) 232.
[19] A.-C. Dupuis, Prog. Mater. Sci. 50 (2005) 929.
[20] R. Khare, S. Bose, J. Miner. Mater. Charact. Eng. 4 (2005) 31.
[21] R.T.K. Baker, Encyclopedia of Materials: Science and Technology, Elsevier, 2005, p. 932.
[22] D.W. Goodman, R.D. Kelley, T.E. Madey, J.T. Yates, J. Catal. 63 (1980) 226.
[23] J. Nakamura, H. Hirano, M. Xie, I. Matsuo, T. Yamada, K. Tanaka, Surf. Sci. 222 (1989) L809.
[24] R.T. Yang, J.P. Chen, J. Catal. 115 (1989) 52.
[25] S. Subramoney, Adv. Mater. 10 (1998) 1157.
[26] S. Brunauer, P.H. Emmett, E. Teller, J. Am. Chem. Soc. 60 (1938) 309.
[27] A. Züttel, Mater. Today (2003) 23.
[28] M.G. Nijkamp, J.E.M.J. Raaymakers, A.J. van Dillen, K.P. de Jong, Appl. Phys. A 72 (2001) 619.
[29] Th. Heine, L. Zhechkov, G. Seifert, Phys. Chem. Chem. Phys. 6 (2004) 980.
[30] F.E. Pinkerton, B.G. Wicke, C.H. Olk, G.G. Tibbetts, G.P. Meisner, M.S. Meyer, J.F. Herbst, J. Phys. Chem. B 104 (2000) 9460.
[31] H. Selig, L.B. Ebert, Adv. Inorg. Chem. Radiochem. 23 (1980) 281.
[32] P.C. Ecklung, NATO ASI-Series, Series B 148 (Intercalation Layered Materials), 1986, p. 309.
[33] M.G. Nijkamp, Ph.D. Thesis, University Utrecht, 2002.
[34] F. Darkrim, D. Levesque, J. Chem. Phys. 109 (1998) 4981.
[35] M. Rzepka, P. Lamp, M.A. de la Casa-lillo, J. Phys. Chem. B 102 (1998) 10894.
[36] Q. Wang, J.K. Johnson, J. Phys. Chem. B 103 (1999) 277.
[37] K. Umemoto, S. Saito, S. Berber, D. Tomanek, Phys. Rev. B 64 (2001) 193409.
[38] D. Tománek, S. Berber, K. Umemoto, S. Saito, Mol. Cryst. Liq. Cryst. 386 (2002) 189.
[39] J.H. Satcher Jr., Th.F. Baumann, J.L. Herberg, R.S. Maxwell, DOE Hydrogen Program, FY 2005 Progress Report.
[40] Y. Okamoto, Y. Miyamoto, J. Phys. Chem. B 105 (2001) 3470.
[41] A.J. Kidnay, M.J. Hiza, Adv. Cryog. Eng. 12 (1967) 730.
[42] I. Cabosso, DOE Hydrogen Program, FY 2005 Progress Report.
[43] A.C. Dillon, K.M. Jones, T.A. Bekkedahl, C.H. Kiang, D.S. Bethune, M.J. Heben, Nature 386 (1997) 377.
[44] D. Levesque, A. Gicquel, F.L. Darkrim, S.B. Kayiran, J. Phys. Condens. Matter 14 (2002) 9285.
[45] G. Stan, M. Cole, J. Low Temp. Phys. 110 (1998) 539.
[46] L. Schlappach, A. Zuettel, Nature 414 (2001) 353.
[47] K.A. Williams, P.E. Eklund, Chem. Phys. Lett. 320 (2000) 352.
[48] M.R. Pederson, J.Q. Broughton, Phys. Rev. Lett. 69 (1992) 2689.
[49] N. Textier-Mandoki, J. Dentzer, T. Piquero, S. Saadallah, P. David, C. Vix-Guterl, Carbon 42 (2001) 2744.
[50] P.A. Cahill, C.M. Rohlfing, Tetrahedron 52 (1996) 5247.
[51] C.C. Henderson, C.M. Rohlfing, P.A. Cahill, Chem. Phys. Lett. 213 (1993) 383.

[52] C. Jin, R. Hettich, R. Compton, D. Joyce, J. Blencoe, T. Burch, J. Phys. Chem. 98 (1994) 4215.
[53] A.I. Kolesnikov, V.E. Antonov, I.O. Bashkin, J.-C. Li, A.P. Moravsky, E.G. Ponyatovsky, J. Tomkinson, Physica (Amsterdam) 263B (1999) 436.
[54] C. Liu, Y.Y. Fan, M. Liu, H.T. Cong, H.M. Cheng, M.S. Dresselhaus, Science 286 (1999) 1127.
[55] S.M. Lee, K.H. An, Y.H. Lee, G. Seifert, Th. Frauenheim, J. Am. Chem. Soc. 123 (2001) 5059.
[56] S.M. Lee, Y.H. Lee, Appl. Phys. Lett. 76 (2000) 2877.
[57] S.-P. Chan, G. Chen, X.G. Gong, Z.-F. Liu, Phys. Rev. Lett. 87 (2001).
[58] J.K. Johnson, V. Simonyan, American Institute of Chemical Engineers Annual Meeting, 1999, paper 21d.
[59] R. Zidan, A.M. Rao, DOE Hydrogen Program, FY 2002 Progress Report.
[60] G.J. Kubas, J. Organomet. Chem. 635 (2001) 37.
[61] P. Chen, X. Wu, J. Lin, K.L. Tan, Science 285 (1999) 91.
[62] S.M. Lipka, Electrochemical Hydrogen Storage and Capture on DOE/NSF-EPSCoR Conference 2004, June 14–16, Argonne National Laboratory, 2004.
[63] C. Carptis, W. Peschka, Int. J. Hydrogen Energy 5 (1980) 539.
[64] J.A. Schwarz, Activated carbon based storage systems, in: Proceedings of the 1992 DOE/NREL Hydrogen Program Review, Honolulu, HI, 1992, p. 271.
[65] A.C. Dillon, M.J. Heben, Appl. Phys. A 72 (2001) 133.
[66] J.E. Fischer, DOE Hydrogen Program, FY 2005 Progress Report.
[67] M. Hirscher, M. Becher, M. Haluka, F. von Zeppelin, X. Chen, U. Detlaff-Weglikowska, S. Roth, J. Alloys Compd. 356 (2003) 433.
[68] S. Orimo, G. Majer, T. Fukunaga, A. Züttel, L. Schlappbach, H. Fujii, Appl. Phys. Lett. 75 (1999) 3093.
[69] G. Seifert, personal communication;
See also: M. Francke, H. Hermann, R. Wenzel, G. Seifert, K. Wetzig, Carbon 43 (2005) 1204–1212.
[70] F. Darkim, J. Vermesse, P. Malbrunot, D. Levesque, J. Chem. Phys. 110 (1999) 4020.
[71] B.C. Hathorn, B.G. Sumpter, D.W. Noid, Phys. Rev. A 64 (2001) 022903.
[72] R.F. Cracknell, Mol. Phys. 100 (2002) 2079.
[73] T. Lu, E.M. Goldfield, S.K. Grey, J. Phys. Chem. B 107 (2003) 12989.
[74] P. Piseri, E. Barborini, M. Marino, P. Milani, C. Lenardi, L. Zoppi, L. Colombo, J. Phys. Chem. B 108 (2004) 5157.
[75] J.S. Arellano, L.M. Molina, A. Rubio, J.A. Alonso, J. Chem. Phys. 112 (2000) 8114.
[76] Y. Okamoto, Y. Miyamoto, J. Phys. Chem. B 105 (2001) 3470.
[77] F. Tran, J. Weber, T.A. Wesolowski, F. Cheikh, Y. Ellinger, F. Pauzat, J. Phys. Chem. 106 (2002) 8689.
[78] O. Hübner, A. Glöss, M. Fichtner, W.J. Klopper, Phys. Chem. A 108 (2004) 3019.
[79] W.-Q. Deng, X. Xu, W.A. Godard, Phys. Rev. Lett. 92 (2004) 1666193.
[80] T. Heine, L. Zhechkov, G. Seifert, Phys. Chem. Chem. Phys. 6 (2004) 980.
[81] Q.U. Wang, J.K. Johnson, J.Q. Broughton, Mol. Phys. 89 (1996) 1105.
[82] Q.U. Wang, J.K. Johnson, Mol. Phys. 95 (1998) 299.
[83] C. Gu, G.-H. Gao, Phys. Chem. Chem. Phys. 4 (2002) 4700.
[84] S. Patchkovskii, J.S. Tse, S.N. Yurchenko, L. Zhechkov, Th. Heine, G. Seifert, Proc. Natl. Acad. Sci. U.S.A. 102 (2005) 10439.
[85] T. Enoki, M. Suzuki, M. Endo, Graphite Intercalation Compounds and Applications, Oxford University Press, Oxford, 2003.
[86] T. Abe, Y. Mizutani, N. Kawabata, M. Inaba, Z. Ogumi, Synth. Met. 125 (2002) 249.
[87] M. Inagaki, O. Tanaike, Carbon 39 (2001) 1083.
[88] C.Q. Fan, DOE Hydrogen Program, FY 2005 Progress Report.
[89] D.D.L. Chung, Encyclopedia of Materials: Science and Technology, Elsevier, 2001, p. 3641.
[90] W.-Q. Deng, X. Xu, W.A. Goddard, Phys. Rev. Lett. 92 (2004) 166103-1.
[91] G. Seifert, J. Schulte, Phys. Lett. A 188 (1994) 364.
[92] J. Chatt, L. Duncanson, J. Chem. Soc. (1953) 2939.
[93] Y. Zhao, Y.-H. Kim, A.C. Dillon, M.J. Heben, S.B. Zhang, Annual American Physical Society meeting March 2006. Los Angeles, (USA) March (2005) 2125.
[94] T. Yildirim, J. Iniguez, S. Ciraci, Phys. Rev. B 72 (2005) 153403.
[95] A.C. Dillon, P.A. Parilla, T. Gennet, K.E.H. Gilbert, J.L. Blackburn, Y.-H. Kim, Y. Zhao, S.B. Zhang, J.L. Alleman, K.M. Jones, T. McDonald, M. Heben, DOE Hydrogen Program, FY 2004 Progress Report.
[96] G.J. Kubas, R.R. Ryan, B.N. Swanson, P.J. Vergatini, J. Wasserman, J. Am. Chem. Soc. 106 (1988) 120.
[97] K. Komatsu, M. Murata, Y. Murata, Science 307 (2005) 238.
[98] Y. Ye, C.C. Ahn, C. Whitam, B. Fultz, L. Liu, A.G. Rinzler, D. Colbert, K.A. Smith, R.E. Smalley, J. Appl. Phys. Lett. 74 (1999) 2307.
[99] C. Liu, Y.Y. Fan, M. Liu, H.T. Cong, H.M. Cheng, M. Dresselhaus, Science 286 (1999) 1127.
[100] R. Chahine, P. Bénard, IEA Task 12: Metal Hydrides and Carbon for Hydrogen Storage, 2001.
[101] R.G. Ding, J.J. Finnerty, Z.H. Zhu, Z.F. Yan, G.Q. Lu, in: H.S. Nalwa (Ed.), Encyclopedia of Nanoscience and Nanotechnology, vol. X, Am. Science Publishers, 2004, pp. 1–21.
[102] A.C. Dillon, T. Gennet, J.L. Alleman, K.M. Jones, P.A. Parilla, M.J. Heben, DOE Hydrogen Program, FY 1999 Progress Report.
[103] C. Liu, Q.H. Yang, Y. Tong, H.T. Cong, H.M. Cheng, Appl. Phys. Lett. 80 (2002) 2389.
[104] X. Chen, U. Detlaff-Weglikowska, M. Haluska, M. Hulman, S. Roth, M. Hirscher, M. Becher, Mater. Res. Soc. Symp. Proc. 706 (2002) 295.
[105] X.B. Wu, P. Chen, J. Lin, K.L. Tan, Int. J. Hydrogen Energy 25 (1999) 261.
[106] M.R. Smith, E.W. Bittner, W. Shi, J.K. Johnson, B.C. Bockrath, J. Phys. Chem. B 107 (2003) 3752.
[107] A.C. Dillon, T. Gennet, J.L. Alleman, K.M. Jones, P.A. Parilla, M. Heben, DOE Hydrogen Program, FY 2000 Progress Report.
[108] M. Hirscher, M. Becher, M. Haluska, U. Detlaff-Weglikowska, A. Quintel, G.S. Duesberg, Y.M. Coi, P. Downes, M. Hulman, S. Roth, I. Stepanek, P. Bernier, Appl. Phys. A 72 (2001) 129.
[109] M. Hirscher, M. Becher, M. Haluska, A. Quintel, V. Skakalova, Y.M. Coi, U. Detlaff-Weglikowska, S. Roth, I. Stepanek, P. Bernier, A. Leonhardt, J. Fink, J. Alloys Compd. 330–332 (2001) 654.
[110] R. Zidan, A.M. Rao, DOE Hydrogen Program, FY 2002 Progress Report.
[111] R.T. Yang, Carbon 38 (2000) 623.
[112] M. Ritschel, M. Uhlemann, O. Gutfleisch, A. Leonhardt, A. Graff, C. Taschner, J. Fink, Appl. Phys. Lett. 80 (2002) 2985.
[113] R.G. Ding, G.Q. Lu, Z.F. Lan, unpublished results, 2003.
[114] C.D.W. Adu, G.U. Sumanasekara, B.K. Pradhan, H.E. Romero, P.C. Eklund, Chem. Phys. Lett. 337 (2001) 31.
[115] B.K. Pradhan, A. Harutyunyan, D. Stojkovic, P. Zhang, M.W. Cole, V. Crespi, H. Goto, J. Fujiwara, P.C. Eklund, Mater. Res. Soc. Symp. Proc. 706 (2002) 331.
[116] H. Zhu, A. Cao, X. Li, C. Xu, Z. Mao, D. Ruan, J. Liang, D. Wu, Appl. Surf. Sci. 178 (2001) 50.
[117] A. Cao, H. Zhu, X. Zhang, X. Li, D. Ruan, C. Xu, B. Wei, L. Liang, D. Wu, Chem. Phys. Lett. 342 (2001) 510.
[118] Y. Chen, D.T. Shaw, X.D. Bai, E.G. Wang, C. Lund, W.M. Lu, D.D.L. Chung, Appl. Phys. Lett. 78 (2001) 2128.
[119] A. Badzian, T. Badzian, E. Breval, A. Piotrowski, Thin Solid Films 398–399 (2001) 170.
[120] N. Nishimiya, H. Ishigaki, H. Takikawa, M. Ikeda, Y. Hibi, T. Sakakibara, A. Matsumoto, K. Tsutsumi, J. Alloys Compd. 339 (2002) 275.
[121] G.G. Tibbetts, G.P. Meisner, C.H. Olk, Carbon 39 (2001) 2291.
[122] H. Lee, Y.S. Kang, S.H. Kim, J.Y. Lee, Appl. Phys. Lett. 80 (2002) 577.
[123] A.D. Lueking, R.T. Yang, AIChE J. 49 (2003) 1556.
[124] X. Li, H. Zhu, L. Ci, C. Xu, Z. Mao, B. Wei, L. Ji, D. Wu, Carbon 39 (2002) 2077.
[125] P. Hou, Q. Yang, S. Bai, S. Xu, M. Liu, H. Cheng, J. Phys. Chem. B 106 (2002) 963.
[126] G. Seifert, Solid State Ionics 168 (2004) 265.
[127] S.M. Lee, K.H. An, G. Seifert, Th. Fraunheim, J. Korean Phys. Soc. 38 (2001) 686.
[128] C.C. Ahn, J.J. Vajo, R. Yazami, D.W. Brown, R.C. Bowman Jr., DOE Hydrogen Program, FY 2002 Progress Report.

[129] A. Züttel, P. Sudan, Ph. Mauton, T. Kiyobayashi, Ch. Emmenegger, L. Schlapbach, Int. J. Hydrogen Energy 27/2 (2001) 203.
[130] S.-P. Chan, G. Chen, X.G. Gong, Z.-F. Liu, Phys. Rev. Lett. 97 (2001) i.
[131] S.M. Lee, Y.H. Lee, Appl. Phys. Lett. 76 (2000).
[132] C. Park, P.E. Anderson, A. Chambers, S.D. Tan, R. Hidalgo, N.M. Rodriguez, J. Phys. Chem. B 103 (1999) 10572.
[133] T. Yildirim, S. Ciraci, Phys. Rev. Lett. 94 (2005) 175501.
[134] P. Guay, B.L. Stansfield, A. Rochefort, Carbon 42 (2004) 2187.
[135] M. Felderhoff, K. Klementiev, G. Grünert, B. Spliethoff, B. Tesche, J.M. Bellosta von Colbe, B. Bogdanovic, M. Härtel, A. Pommerin, F. Schüth, C. Weidenthaler, Phys. Chem. Chem. Phys. 6 (2004) 4369.
[136] Z. Dehouche, L. Lafi, N. Grimard, J. Goyette, R. Chahine, Nanotechnology 16 (2005) 402–409.
[137] C.C. Ahn, Y. Ye, B.V. Ratnakumar, C. Witham, R.C. Bowman Jr., B. Fultz, Appl. Phys. Lett. 73 (1998) 3378.
[138] D.J. Browning, M.L. Gerrard, J.B. Lakeman, I.M. Mellor, R.J. Mortimer, M.C. Turpin, in: Z.Q. Mao, T.N. Veziroglu (Eds.), Hydrogen Energy Progress XIII, Proceedings of the 13th World Hydrogen Energy Conference, Beijing, June 11–15, 2000, pp. 554–559.
[139] E. Poirier, R. Chahin, T.K. Bose, Int. J. Hydrogen Energy 26 (2001) 831.
[140] M.A. de la Casa-Lillo, F. Lamari-Darkrim, D. Cazorla-Amoros, A. Linares-Solano, J. Phys. Chem. B 106 (2002) 10930.
[141] J.Y. Hwang, S.H. Lee, K.S. Sim, J.W. Kim, Synth. Met. 126 (2002) 81.
[142] M. Hirscher, M. Becher, J. Nanosci. Nanotechnol. 3 (2003) 3.
[143] R. Ströbel, L. Jörissen, T. Schliermann, V. Trapp, W. Schütz, K. Bohnhammel, G. Wolf, J. Garche, J. Power Sources 84 (1999) 221.
[144] B.K. Gupta, O.N. Srivastava, Int. J. Hydrogen Energy 25 (2000) 825.
[145] B.K. Gupta, O.N. Srivastava, Int. J. Hydrogen Energy 26 (2001) 857.
[146] Y.Y. Fan, B. Liao, M. Liu, Y.L. Wei, M.Q. Lu, H.M. Cheng, Carbon 37 (1999) 1649.
[147] H.M. Cheng, C. Liu, Y.Y. Fan, F. Li, G. Su, L.L. He, M. Liu, Z. Metallkd. 91 (2000) 306.
[148] S. Hill, New Sci. (1996) 20.
[149] A. Chambers, P. Colin, R.T.K. Baker, N.M. Rodriguez, J. Phys. Chem. B 102 (1998) 2251.
[150] In [1], private communication with I.M. Mellor, University of Lougborough/DERA, UK.
[151] A.D. Lueking, R.T. Yang, N.M. Rodriguez, R.T.K. Baker, Langmuir 20 (2004) 714.
[152] R. Ströbel, Ph.D. Thesis, Technical University Freiberg, March 2005.
[153] A. Lueking, R.T. Yang, AIChE J. 49 (2003) 1556.
[154] J. Lachawiec, G. Qi, R.T. Yang, Langmuir, submitted for publication; R.T. Yang, J. Lachawiec, G. Qi, U.S. DOE, Hydrogen Program Review 2005, VI.C.11 University of Michigan.
[155] C. Nutzenadel, A. Zuttel, D. Chartouni, L. Schlapbach, Electrochem. Solid-State Lett. 2 (1) (1999) 30.
[156] K. Jurewicz, E. Frackowiak, F. Béguin, Electrochem. Solid-State Lett. 4 (2001) A27.
[157] X. Qin, X.P. Gao, H. Liu, H.T. Yuan, D.Y. Yan, W.L. Gong, D.Y. Song, Electrochem. Solid-State Lett. 3 (2000) 532.
[158] S.M. Lee, K.S. Park, Y.C. Choi, Y.S. Park, J.M. Bok, D.J. Bae, K.S. Nahm, Y.G. Choi, S.Ch. Yu, N. Kim, T. Frauenheim, Y.H. Lee, Synth. Met. 113 (2000) 209.
[159] N. Rajalakshmi, K.S. Dhathathreyan, A. Govindaraj, B.C. Satishkumar, Electrochim. Acta 45 (2000) 4511.
[160] H.S. Youn, H. Ryu, T.H. Cho, W.K. Choi, Int. J. Hydrogen Energy 27 (2002) 937.
[161] G. Dai, M. Liu, D. Chen, P. Hou, Y. Tong, H.M. Cheng, Electrochem. Solid-State Lett. 5 (2002) E13.
[162] X.P. Gao, Y. Lan, G.L. Pan, F. Wu, J.Q. Qu, D.Y. Song, P.W. Shen, Electrochem. Solid-State Lett. 4 (2001) A173.
[163] X. Yan, X. Gao, Y. Li, Z. Liu, F. Wu, Y. Shen, D. Song, Chem. Phys. Lett. 372 (2003) 336.
[164] J.M. Skowronski, P. Scharff, N. Pfander, S. Cui, Adv. Mater. 15 (1) (2003) 55.
[165] X. Chen, Y. Zhang, X.P. Gao, G.L. Pan, X.Y. Jiang, J.Q. Qu, F. Wu, J. Yan, D.Y. Song, Int. J. Hydrogen Energy 29 (2004) 743.
[166] J. Liu, Z. Mao, D. Hao, X. Xie, D. Wu, Presented at 204th ECS Meeting, Orlando, FL, October 12–16, 2003 (Abstract, 130).
[167] G.P. Dai, C. Liu, M. Liu, M.Z. Wang, H.M. Cheng, Nano Lett. 2 (5) (2002) 503.
[168] I. Lombardi, M. Bestetti, C. Mazzocchia, P.L. Cavallotti, U. Ducati, Electrochem. Solid-State Lett. 7 (2004) A115.
[169] S.M. Lee, K.H. An, W.S. Kim, Y.H. Lee, Y.S. Park, G. Seifert, Th. Frauenheim, Synth. Met. 121 (2001) 1189.
[170] R.T. Yang, Carbon 38 (2000) 623.
[171] J. Milliken, J. Petrovic, W. Podolski, International Workshop on Hydrogen Matter & Vacuum Systems, Newport News, VA, November 11–13, 2002.
[172] Y.M. Malozovsky, V. Subramanian, T. Reese, B. Rambabu, Louisiana Conference on Commercial Application of Microsystems, Materials and Nanotechnologies, Louisiana, October 21–22, 2002.
[173] R.E. McAlsiter, www.ahanw.org/library/storage/safestorage.php.
[174] A.C. Dillon, P.A. Parilla, Y. Zhao, Y.-H. Kim, T. Gennett, C. Curtis, J.L. Blackburn, K.E.H. Gilbert, J.L. Alleman, K.M. Jones, S.B. Zhang, M.J. Heben, Proceedings of U.S. DOE, Hydrogen Program Review, 2005.
[175] IPHE Scoping Paper Overview, the Secretariat of the Implementation and Liaison Committee of the IPHE, Washington, 2004.
[176] A.C. Dillon, K.E. Gilbert, P.A. Parilla, A. Alleman, G.L. Hornyak, K.M. Jones, M.J. Heben, Proceedings of U.S. DOE, Hydrogen Program Review, 2002.